An Analytical Study of Radon Concentration in Water from Some Rivers in Gauteng using a solid-state $\alpha-$Detector

A thesis submitted in fulfilment of the
requirements for the Degree of
MPhil Nuclear Energy Studies

by

Livhuwani Masevhe

University of Johannesburg

2017

An Analytical Study of Radon Concentration in Water from Some Rivers in Gauteng using a solid-state $\alpha-$Detector

Livhuwani Masevhe

201281808

SUPERVISORS:

Dr. Mavunda, RD

University of Johannesburg (UJ)

South African Nuclear Energy Corporation (NECSA)

Prof. Connell, SH

University of Johannesburg (UJ)

A thesis submitted in fulfillment of the requirements for the degree of Master of Philosphy (MPhil) in Nuclear Energy Studies

The University of Johannesburg

PO Box 524

Auckland Park, 2006

REPUBLIC OF SOUTH AFRICA

Declaration

I, the undersigned, hereby declare that this work is my own. The work in this thesis is my original work and it has not been submitted before for any degree or examination at any University.

.....

Livhuwani Masevhe (Candidate)

.....

Date

Abstract

In view of the geological arrangement and the long historic activities of gold mining in the Gauteng Province in South Africa, uranium bearing minerals have been exposed at or near the surface. The mine dumps around the gold mines in the Gauteng Province were assumed to be potentially hazardous and contain elevated levels of naturally occurring radioactive materials (NORM). There is a potential increase of radon in the area, since the soil in the mine dumps contains radium-226 (the parent radioisotope of radon-222) and it could pollute the nearby rivers and streams. Rivers running towards West and South of the Gauteng province originates mainly from the mining areas whilst those running towards the East and North of the Province are not necessarily originating from the mining areas.

The current study was carried out to determine the level of radon and the possible over exposure of the public to radon concentrations from twenty-five rivers and tributaries in Gauteng Province. Fifty water samples were collected from different regions of the province including those areas around the mine dumps and those that are far but in the residential areas. The samples were analyzed for radon concentration. Three different brands of commercially available water were also studied. Due to its reliability for laboratory and field determination of radon concentrations in the current study, the alpha-spectrometry ($\alpha-$spectrometry) technique was applied using RAD-7 instrument.

Standard water samples were used to calibrate the detector of choice in this study, and the Liquid Scintillation Counter (LSC) was used as a reference detector. The $\alpha-$spectrometry method was optimized to count the $\alpha-$particles emitted by ^{218}Po and ^{214}Po in secular equilibrium with their parent, ^{222}Rn. The variation of radon

concentrations as a function of sample's volume, height, temperature, counting time, seasons and meteorological data were studied. The exercise showed the theory of meteorological parameters which influence the effect of radon concentration agreed well with the measurements and confirmed the good functionality of the detector.

The measurements showed that the radon concentrations from the North and the North-East rivers were slightly higher with Moretela river having the highest radon concentration of 4.9 ± 0.3 Bq.l^{-1} than the South and the West rivers with the Vaal river having the lowest radon concentration of 0.1 ± 0.1 Bq.l^{-1} in the Gauteng Province. The average radon concentration for the general rivers water survey in Gauteng Province was 1.4 ± 0.2 Bq.l^{-1}. The concentrations of radon in three commercial bottled waters had the values 0.7, 0.3 and 0.2 Bq.l^{-1}. Both river and commercial water radon concentration analysed were found to be below the internationally acceptable levels for radon concentration in water, which are 11.1 Bq.l^{-1} and 100 Bq.l^{-1} for United States Environmental Protection Agency (USEPA) and the World Health Organisation (WHO), respectively. Hence, the average annual dose of radon from Gauteng Province rivers poses no threat to the general public.

An increase in radon concentration was observed downstream mainly in the North East Rivers of the Gauteng Province which was assumed to be due to accumulation of radon from one point of the river to the next emanating from the bedrock. The current study shows that while other NORM isotopes, not as mobile as radon, might show stronger correlation to anthropogenic activities, in surface water radon will be less so. It is not significantly increasing due to anthropogenic activities and it shows natural sources are the most significant for radon.

Acknowledgments

I give all the honour and the glory to God, the Creator of Knowledge in the name of my Saviour Jesus Christ, who gave me courage and strength to complete this study (Philippians 4:13).

It gives me an immense pleasure to express my deep sense of gratitude and indebtedness to my two supervisors Dr. Mavunda, R.D., and Prof. Connell, S.H. for their tireless effort in supervising my thesis amidst their busy schedules. Their scholarly guidance has been immeasurable in light of the detail required for this work. I have learnt various aspects of Radon studies by their stimulating guidance and encouragements at all stages of the work.

I am grateful to the University of Johannesburg (UJ), the South African Nuclear Energy Corporation SOC Ltd (Necsa) and iThemba LABS-Gauteng for not only providing the research and development platform, but also the access to different facilities such as the MSONE Room, Library (UJ), Radiation Protection Training Center (RPTC) and Radio-Analysis Laboratories (Necsa). Thank you to the Vaal University of Technology (VUT) for the recognition of my studies. The financial assistance by the National Research Foundation (NRF) which was provided funding for my studying is greatly appreciated.

Finally, my dear Wife: Thilivhali Masevhe. Long way's journey, prove your love and support during the entire course of this work. Special thanks to my daughters Bono and Wamashudu, and son Akonaho: your existence continue to inspire me in my work and my life.

Table of Contents

List of Figures

List of Tables

1 Background

1.1 Radon and its Significance

The exposure to excessive radiation from radon due to its radioactivity, has drawn the attention of many scientists all over the world, particularly in the last decade [1]. Generally, an important research goal has been the evaluation of the indoor radon concentration, essentially because radon is the most relevant source of the major mean public exposure to ionizing radiation [2]. Radon (^{222}Rn) and its progeny is the highest exposure of all the natural radionuclides to which human beings in the general environment are exposed [4]. It is a progeny of radium (^{226}Ra) which is found in the uranium (^{238}U) decay chain; it can enter the human body through ingestion when consuming food or water which is contaminated with radon, or by breathing in radon-filled air [3].

During inhalation, radon progeny can be trapped in the lungs. During the decay process of radon, it releases the energy which can be diposited in the surrounding tissue in the lungs [5] or its decay products can be transported by the blood vessels to other organs where it causes chromosomal aberrations leading to higher chance of cancer incidence [6]. Therefore, any radon inhaled or ingested becomes a health problem, hence the measurement of radon concentrations in the environment is of special interest to mankind. Further epidemiological studies and analyses of radon exposure again confirmed clear evidence that lung cancer can be caused by exposure to radon gas [7].

Many studies on radon concentration in natural water sources such as groundwater, boreholes, surface water or rivers have been conducted throughout the world,

however, more still need to be done in most of the South African rivers. Rivers in the country are used, among others, for agricultural and household purposes due to the scarcity of water. This behavior can expose the general public to the elevated levels of NORMS that are formed due to the geological set-up of the area. Looking at the landscape of the Gauteng Province, and its historical gold mining activities, there could be higher chances of excess NORMS in the area. The mining activities impact the environment badly due to among other effects, the contamination of the water resources, which has the potential to threaten or affect the health of nearby communities even many years after the mine is closed.

The current study focus on the surface water or rivers that flow close to the mine dumps in in the Gauteng Province. The mine dumps around the gold mines are a likely the source of radon (^{222}Rn), since the soil in the dumps contains radium activity concentrations of typically 200 to 300 Bq.kg^{-1} [15]. Based on this background, an elevated concentrations of radon in the rivers that originate from the mine dumps and the surrounding areas are expected, leading to an urgent need for its assessment. A.T.A. Siddig and R. Lindsay (UWC 2009), noted that, "because of its nature which is a noble gas, radon can easily escape from mineral surfaces and dissolve in groundwater, which can carry it away from its point of origin. Radon is rarely found in significant concentrations in river water, due to its rapid dispersal into the atmosphere" [53].Therefore, the concentrations of radon is expected to subside as the rivers flow away from the city. Besides monitoring radon concentration levels in water, the effects of meteorological parameters were taken into consideration to understand their contribution to the radon exhalation from the water to the atmosphere. It is against this background that the current study was conducted.

1.2 Motivation for this Study

Water is fundamental to life on earth, and, therefore is one of the most valuable resources. Clean water remains a major challenge facing modern civilization and many people are still using natural water. The challenges include the securing of natural water systems and the mitigation of on-going, detrimental effects of the

modern world, especially in the face of climate change and population growth [16]. Radioactivity, (^{222}Rn)in particular is present in natural water as a result of natural processes or from the mining and the production or disposal of radioactive materials [16]. According to the World Health Organisation (WHO), the simultaneously measured activity of radionuclide-specific concentrations of natural $\alpha-$emitters should comply with the guideline levels set by WHO which are 10 Bq.l^{-1} for ^{238}U and 100 for Bq.l^{-1} (^{222}Rn) [18]. The United States Environmental Protection Agency (USEPA) has recommended a radon limit in water of 11.1 Bq.l^{-1} [19].

In South Africa the studies of radon concentration in different types of water such as grownwater, boreholes and few rivers have been carried out over the past decade. However, the studies that were conducted to measure the quality of water from the mines, particularly in the Gauteng and the North West Provinces paid little attention to radon concentration. Those studies include a PhD research by Siddig Abdalla Talha (UWC 2009) to investigate and develop radon-in-water measuring methods applicable to aquifers and rivers using a hyper-pure germanium (HPGe) detector [53] in the Gauteng province, South Africa. Furthermore, the Department of Water Affairs and Forestry (DWAF) in 2003 conducted a study to monitor the levels of radioactivity in the Klip River. The river originates from the area where there are mine dumps that are situated in Johannesburg south of the Witwatersrand and it flows through the Soweto Township towards the south into the Vaal River in Vereeniging. The study was done to determine the total radioactivity dose from surface and some groundwater sources that could be used potentially as drinking water supplies [20]. The results revealed that all the samples from the river had the lifetime average annual radiation dose below 1.0 mSv.a^{-1}, "which implied that no radiological problem exists from the viewpoint of drinking water" [20].

GDARD (2012), a study conducted by the Gauteng Department of Agriculture and Development found that, "the presence of radioactivity in the mine residue areas (MRAs) in Gauteng. These elements are found, in trace amounts, in almost all types of soil and rocks. According to the database compiled during Phase 1 of

the project (GDARD, 2009), it was assumed that all gold MRAs are radioactive. The concentration of radioactive MRAs in the Witwatersrand headwater areas of the Vaal catchment is evident, with some overlapping into the Limpopo (Crocodile West) headwaters near Krugersdorp" [81].

In view of the previous studies of radon in water and the background given, the current study was done to broaden the scope and determine whether radon-222 concentration in the rivers from the mining activities is elevated. This was done by measuring for radon concentration from the rivers flowing from the areas with mine dumps and also those that are far from the dumps. The water quality from those rivers river were compared with the international acceptable standards. Due to the dense population in the province, most of the residences are located close to the rivers. The study covers mainly surface streams from different parts of the province. To estimate the health risk posed by radon in water and to use it as a decision making tool, a systematic approach was adapted for this research project [20].

1.3 Objectives of this Study

The proposed research work envisaged a study of the environmental radioactivity in the Gauteng Province, South Africa with specific attention to the measurements of radon in water and its progeny levels in some rivers and their impact on health.

The major objectives of the present research work are:

a) To assess the level of radon concentration in the rivers that are around the mining activities as compared to those that are remote from (the possibility of draining) mining activities;

b) To assess the exposure of radiology to the public living in the Gauteng Province due to Naturally Occurring Radioactive Materials (NORM) as a result of the mining activities;

c) To develop a reliable measurement of radon activity concentrations in water by using an $\alpha-$spectrometry technique:

   i) by comparing the results of analyses from the more recent and robust technique based on $\alpha-$spectrometry using the solid-state $\alpha-$detector;

   ii) by verifying the effects of meteorological parameters such as the sample temperature, volume and concentration on the radon release-rate and radon content in the samples; and

   iii) calibrating the detector of choice with another reference detector by measuring the standard sample prepared from the laboratory.

1.4 Organization of this Thesis

This thesis comprises of six chapters. Chapter 1 introduces the context and the objectives of this study. Chapter 2 begins with a summary of previous studies of radon in water which further details the hypothesis of the current study. The characteristics of radon gas and its properties, the isotopes of radon and the decay chains involved are described in this chapter which also covers the origin of radon and its propagation in nature further. Chapter 2 also delineates the basic principles of radon detection, measurement techniques and methods used for radon detection in natural water, general transport theory and different types of detectors. Chapter 2 then continues with discussions concerning radon detectors and the measurement of radon in water. Chapter 3 discusses the experimental aspects of measuring radon in this work. Chapter 4 covers analyses which include radioactive counting and numerical analysis. The experimental results are presented in Chapter 5. Discussions of the findings and the conclusion are elaborated on in Chapter 6 and Chapter 7, respectively.

2 Literature Review and Contextual Discussion

2.1 Studies of Radon in Water

Many studies have been done on radon, radium and other radionuclides in different types water around the world [12]. O. Maxwell *et al.* (2014), noted that, "the groundwater reacts with the ground and bedrock, releasing dissolved compounds which depend on the geochemical composition of the soil and rock, as well as the residence time of the groundwater in the soil and bedrock" [23]. Some groundwater pollution occurs naturally when radium enters groundwater by a number of processes including the decay of dissolved parent isotopes and alpha-recoil [24]. Radium decays and produces a radioactive radon gas. Groundwater can surface from springs or it can discharge into lakes, streams, rivers or oceans [24]. When groundwater meets the river, the water will enter the river and continue flowing downstream as surface water. Guidelines and policies on radionuclides in drinking water have been published internationally [24]. The United Nations Scientific Committee on the Effects of Atomic Radiation (UNSCEAR) recommended that the radon concentration in the water must be between 4 and 40 mBq.l^{-1} [79].

Over a decade, many methods have been developed to measure the radon concentration in water including an $\alpha-$spectrometry approach throughout the world. This technique has been the most preferred in the analyses of radon concentration in soil, water and air. However, a lot of publications are mainly on measured values and less on meteorological effects and quality control issues as far as the radon release rate from the medium to the atmosphere is concerned. The emanation of

radon from the water has been studied in detail by various authors both theoretically and experimentally [80] and the existence of external factors that affect the release of radon to the atmosphere is well established [80].

L. Salonen (Handbook of Radioactivity Analysis, Third Edition, pages 625 – 693, 2012), noted that, "radon in drinking water presents a risk for the development of internal organ, cancers by radiation exposure of cells in the gastrointestinal tract and in other organs once radon is absorbed into the blood stream. In fact, the lung cancer risk from radon in drinking water is higher than that of stomach cancer, which is the most probable compared to other cancers [33]. The radon concentration in surface water is typically less than 4 Bq.l^{-1} while in groundwaters the concentrations vary over a wide range up to 10 kBq.l^{-1} or even higher. The worldwide average annual dose from inhaled radon (1.26 mSv) is about half of the average dose from all natural sources of radiation (2.40 mSv)" [33].

L. Salonen (Handbook of Radioactivity Analysis, Third Edition, pages 625 – 693, 2012), "because radon is an inert gas, it is an excellent tracer either alone or together with radium for studying geochemical, hydrological, and oceanic processes such as groundwater discharge rates, groundwater seepage, gas exchange across the air-water interface as well as mixing processes between groundwater, seawater and submarine groundwater discharges [34, 35, 36, 37]. Radon is also a useful natural tracer in geophysical investigations, as in predicting earthquakes" [33].

2.2 Occurrence of Radon

The concept of Radioactivity and Radon was presented by S. Lorenz (F50/51 Limnophysics, 2011, pages 25 – 26) as, "Figures 2.1a and 2.1b present the three decay series which can be detected and the Thorium series, the Uranium-Radium series and the Uranium-Actinium series [30]. The fourth decay series of the Neptunium, because of its half-life, ($T_{1/2}$), of the starting isotope of 2.14 million years has already almost completely decayed" [30]. In the Figures 2.1a and 2.1b the half-life ($T_{1/2}$) of each radionuclide is indicated in the box (a: years, d: days, m: minutes and s: seconds). ^{222}Rn is in the ^{238}U decay series [27].

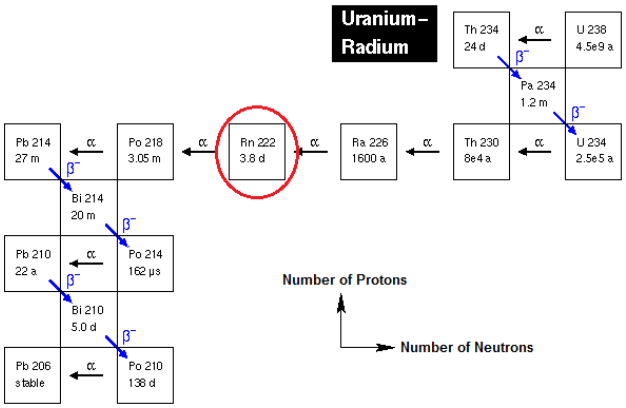

(a) Diagram of the ^{238}U natural decay series [22].

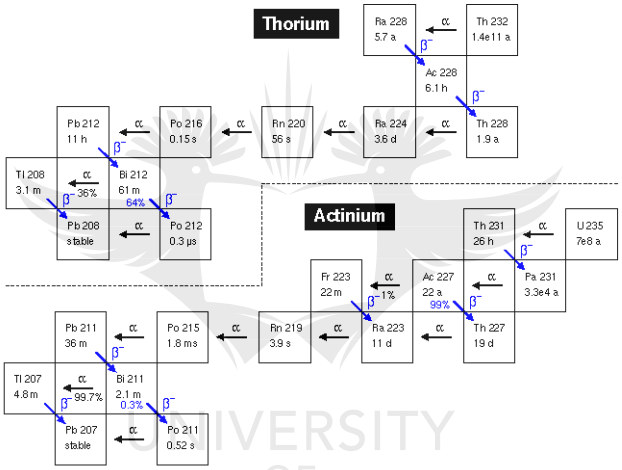

(b) Two natural decay series of ^{232}Th and ^{235}U [22].

Figure 2.1: The three decay series which can be detected and the Thorium series, the Uranium-Radium series and the Uranium-Actinium series [30]

L. Salonen (Handbook of Radioactivity Analysis, Third Edition, pages 625 – 693, 2012) further noted that, "other natural radon isotopes are thoron (^{220}Rn; $T_{1/2} = 55.6$ s) and action (^{219}Rn; $T_{1/2} = 3.96$ s). They arise in the decay series of ^{232}Th and ^{235}U respectively as shown in Figure 2.1b. Uranium and thorium occur in all types of soil and rocks at varying concentrations. They produce radon and thoron which can diffuse from mineral grains into pore spaces and thereafter es-

cape into air and dissolve in water [29]. Because thoron has a much shorter half-life than radon, it can travel much shorter distance before decaying than radon. Therefore, thoron is of concern only where the concentration of ^{232}Th is high [29]. The contribution by the action to airborne radon is insignificant due to its short half-life."

The decay of radium to radon is shown in Figure 2.2. Frank H. Attix indicated that, "when$^{226}_{88}$Ra atom decays, it emits the $\alpha-$particle, its atomic number decreases by 2 and it consequently sheds two atomic electrons from its outermost shell, and it becomes a positively charged ion of $^{222}_{86}$Rn" [28]. The two electrons are captured by the emitted $\alpha-$particle, to form a neutral $^{4}_{2}$He atom [28].

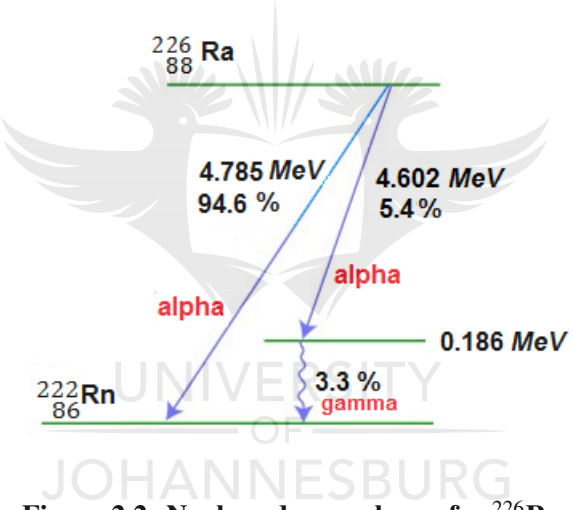

Figure 2.2: Nuclear decay scheme for $^{226}_{88}$Ra.

The disintegration of $^{226}_{88}$Ra results in two branches i.e., one of the branches shows that 94.4 % decays directly to $^{222}_{86}$Rn, making 4.79 MeV available, which is the kinetic energy shared by the $\alpha-$particle (4.70 MeV) and the recoiling $^{222}_{86}$Rn atom (0.085 MeV) [28]. The other branch occurs in 5.5 % of the nuclei, and releases 4.60 MeV of kinetic energy and gives rise to the nuclear excited state of $^{222}_{86}$Rn. This promptly relaxes to the ground state through the emission of a 0.18 MeV $\gamma-$ray [28]. The same total kinetic plus quantum energy is released by either route, and the net reduction atomic rest mass is identical for each [28].

2.3 Radioactivity and Radon

Radioactivity was defined in S. Lorenz (F50/51 Limnophysics, 2011, pages 25 – 26), "the process in which atomic nuclei decay and emit radiation. This phenomenon has been in existence on earth since its creation. An unstable nucleus can decay into a stable nucleus or into another unstable one [30]. Therefore a decay series can arise. Altogether only four different $\alpha-$decay series exist, because $\beta-$ or $\gamma-$decay processes do not change the mass number, but the $\alpha-$decay processes decrease the mass number by four units for each decay" [30].

2.3.1 Alpha Decay ($\alpha-$decay)

Alpha decay was presented well by Kenneth Krane (Introductory Nuclear Physics, pages 161 – 164), "It can be energetically favourable for a heavy nucleus to decay into a lighter nucleus and an $\alpha-$particle, as can be seen by considering the relative binding energies of the parent, daughter and $\alpha-$particle. The $\alpha-$particle can subsequently acquire two electrons to form a helium atom. This process is called an $\alpha-$decay. The $\alpha-$particles do not penetrate far into a material and can be stopped quite easily; however, they are capable of breaking chemical bonds (which can cause chemical or biological damage) when they strike a molecule because of their kinetic energy, mass and charge. Thus, because $\alpha-$particles can be stopped by thin barriers such as a piece of paper or skin, $\alpha-$emitters are mostly damaging if they are ingested or inhaled" [31]. The decay process is:

$$ {}^{A}_{Z}P_{N} \longrightarrow {}^{A-4}_{Z-2}D_{N-2} + {}^{4}_{2}He + Q, \tag{2.1} $$

where P and D are the parent and daughter nuclei, respectively. A is an atomic mass, N is the atomic number or number of neutrons and Z is the number of protons in the nucleus [21]. For $\alpha-$emission to occur, the following conservation equation must be satisfied:

$$ M_P = M_D + m_\alpha + 2m_e + Q, \tag{2.2} $$

where M_P, M_D, m_α and $2m_e$ are the masses of the parent neutral atom, the daugh-

ter neutral atom, the emitted $\alpha-$particle, respectively. The two orbital electrons that are lost during the decay to the lower atomic numbered daughter and Q is the total energy released associated with the radioactive transformation [26]. The exact kinetic energy division between the α and recoil nucleus depends on the mass of the daughter and may be calculated by applying the laws of conservation of energy and momentum [82].

If M and m are respectively the masses of the recoil nucleus and $\alpha-$particles, and V and v are their respective velocities, then

$$Q = \frac{1}{2}MV^2 + \frac{1}{2}mv^2. \tag{2.3}$$

According to the law of conservation of momentum, $MV = mv$, or

$$V = \frac{mv}{M}. \tag{2.4}$$

When the value of V from Equation 2.4 is substituted into Equation 2.3, we have

$$Q = \frac{1}{2}M\frac{m^2v^2}{M^2} + \frac{1}{2}mv^2. \tag{2.5}$$

If E represents the kinetic energy of the $\alpha-$particle, $\frac{1}{2}mv^2$, the $Q-$value in the Equation 2.5 may be written as $Q = E\left(\frac{m}{M}+1\right)$ or " [31]

$$E = \frac{Q}{1+(m/M)}. \tag{2.6}$$

E is slightly less than the $Q-$value, nearly all the energy released in the decay is carried away as kinetic energy by the light particle [82]. Equation 2.6 also shows that in *two-particle* emission from an initially unstable nucleus at rest, the $\alpha-$particle emerges with a *precisely defined energy*; since Q has a precise value, so does E [82].

2.3.2 Radon and its Progeny Decay Energies

The $\alpha-$particle, structured like the nucleus of the helium ($^4_2$He) atom and it has two protons and two neutrons [31]. Figure 2.3 describes the energy that is released during the decay process. The $\alpha-$decay equations of ^{222}Rn, ^{218}Po and ^{214}Po in Equations 2.7 to 2.9:

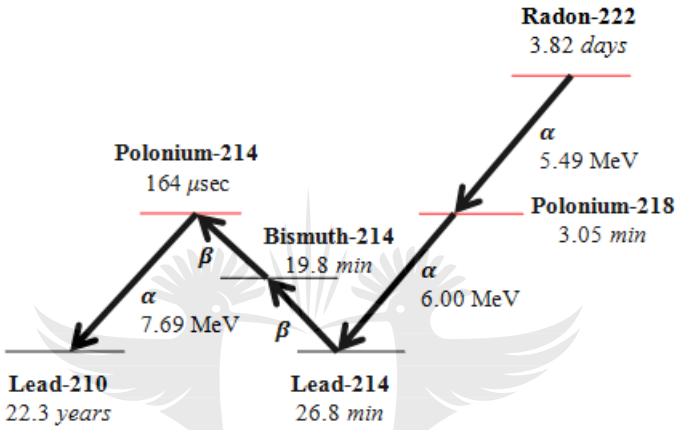

Figure 2.3: Radon decay chain [67].

Important examples are represented by the mass-energy balance equations:

$$^{222}_{86}Rn \longrightarrow {}^{218}_{84}Po + {}^{4}_{2}He + 5.49 \quad MeV, \tag{2.7}$$

$$^{218}_{84}Po \longrightarrow {}^{214}_{82}Po + {}^{4}_{2}He + 6.00 \quad MeV, \tag{2.8}$$

$$^{214}_{80}Po \longrightarrow {}^{210}_{78}Pb + {}^{4}_{2}He + 7.69 \quad MeV. \tag{2.9}$$

F.H. Attix (1986) showed that, "in the radon decay series, the α-particle is emitted by the $^{222}_{86}$Rn atom, its atomic number decreases by 2 and it consequently sheds two atomic electrons from its outermost shell, to become $^{218}_{84}$Po [28]. After the $\alpha-$particle slows down, it captures two electrons from its surroundings, thereby becoming a neutral $^4_2$He atom. The 5.49 MeV shown in the Equation 2.7 is the

energy equivalent of the rest mass decrease in transforming a neutral $^{222}_{86}$Rn into neutral atoms $^{218}_{86}$Po and $^{4}_{2}$He" [28].

The $Q-$value of the decay, is the difference of the mass of the parent neutral atom and the combined mass of the daughter neutral atom, the $\alpha-$particle and two orbital electrons that are lost during the transformation of ^{222}Rn to ^{218}Po [31]. When the nuclide masses are expressed in the more convenient atomic mass units (amu), the energy liberated in decay equations can be calculated in units of mega-electron volts (MeV) according to Equation 2.2 which can be written as [31]:

$$Q_\alpha = (M_{^{222}Rn} - M_{^{218}Po} - m_\alpha - 2m_e) \times (931.494 MeV/amu). \tag{2.10}$$

The precise atomic mass units can be inserted into Equation 2.10 to obtain:

$$\begin{aligned} Q_\alpha &= (222.0176 - 218.0090 - 4.002602) amu \times (931.494 MeV/amu) \\ &= (0.005998) amu \times (931.494 MeV/amu) \\ &\approx 5.49 MeV. \end{aligned} \tag{2.11}$$

The value of 5.49 MeV is the disintegration energy for the decay. It includes the kinetic energy of both the $\alpha-$particle and the heavy recoiling daughter so that the kinetic energy of the alpha particle will be slightly less [2]. Conservation of momentum and energy in this reaction requires that (from Equation 2.6) [2] the kinetic energy of the $\alpha-$particle, E, is:

$$E = \frac{5.49}{1 + \left(\frac{4}{218}\right)} = 5.39 MeV. \tag{2.12}$$

Abdul.R.H.Subber *et al.* (2011) noted that, "the kinetic energies of the emitted alpha particles can be measured very precisely to distinguish between the Q value and the kinetic energy, E. The very small recoil energy of the heavy daughter is very difficult to measure but is still large compared to chemical bond energies and can lead to interesting chemistry. The emitted $\alpha-$particles have discrete energies

from about 4 – 10 MeV, spanning a range of about a factor of 2, but half-lives ranging from 10^{-6} – 10^{17} s, spanning a range of about a factor of 10^{23}. Short-lived $\alpha-$emitters have the highest energies as indicated in the table below" [2].

Table 2.1: Radioactive properties of ^{222}Rn and its short-lived progeny.

$\alpha-$emitter	A (amu)	$T_{1/2}$ (s)	λ (s^{-1})	Q-value (MeV)	E (MeV)
$^{222}_{86}Rn$	222.0176	3.3×10^5	2.1×10^{-6}	5.49	5.39
$^{218}_{84}Po$	218.0090	183	3.8×10^{-3}	6.00	5.89
$^{214}_{80}Po$	213.9920	0.164	2.23	7.69	7.56

2.3.3 Radioactive Decay Chain

Since isolated observation is impossible under normal conditions, it becomes important to model the activity of any member of a decay chain under certain initial conditions. Differential equations, which govern the time evolution of all elements in a radioactive chain form a system known as the Bateman Equations. The basic concept is illustrated using a two-element decay chain where A represents the abundance of the first isotope, which decays into isotope B [45].

$$\frac{dA}{dt} = -\lambda_A N_A, \tag{2.13}$$

$$\frac{dB}{dt} = \lambda_A N_A - \lambda_B N_B. \tag{2.14}$$

The rates of change of the four isotopes in the chain are described by the differential equations

$$\frac{dN_1}{dt} = -\lambda_1 N_1, \tag{2.15}$$

$$\frac{dN_2}{dt} = \lambda_1 N_1 - \lambda_2 N_2, \tag{2.16}$$

$$\frac{dN_3}{dt} = \lambda_2 N_2 - \lambda_3 N_3, \tag{2.17}$$

$$\frac{dN_4}{dt} = \lambda_3 N_3 - \lambda_4 N_4, \tag{2.18}$$

where N_1, N_2, N_3 and N_4 are the number of atoms of the four elements in a decay chain. The decay constant, λ, related to the half-life by $\lambda = \frac{\ln 2}{t_{1/2}}$. This can be extended to decay chains with many elements, and can be solved numerically or analytically to produce results as follow, which is used to predict the rate of $\alpha-$particles emitted [45]:

$$A(t) = A_0 e^{-\lambda_A t}, \tag{2.19}$$

$$B(t) = B_0 e^{-\lambda_B t} + \frac{A\lambda_A}{\lambda_B - \lambda_A}\left(e^{-\lambda_A t} - e^{-\lambda_B t}\right). \tag{2.20}$$

Integrating the differential equations above in Equation 2.15 to Equation 2.18 gives the number of atoms of each isotope as a function of time [47]

$$N_1(t) = N_1 e^{-\lambda_1 t}, \tag{2.21}$$

$$N_2(t) = N_2(0)e^{-\lambda_2 t} + \frac{\lambda_1 N_1(0)}{\lambda_2 - \lambda_1}\left(e^{-\lambda_1 t} - e^{-\lambda_2 t}\right), \tag{2.22}$$

$$\begin{aligned} N_3(t) = N_3(0)e^{-\lambda_3 t} &+ \frac{\lambda_2\lambda_1 N_1(0)}{\lambda_2 - \lambda_1}\left(\frac{e^{-\lambda_1 t} - e^{-\lambda_3 t}}{\lambda_3 - \lambda_1} - \frac{e^{-\lambda_2 t} - e^{-\lambda_3 t}}{\lambda_3 - \lambda_2}\right) \\ &+ \frac{\lambda_2 N_2(0)}{\lambda_3 - \lambda_2}\left(e^{-\lambda_2 t} - e^{-\lambda_3 t}\right), \end{aligned} \tag{2.23}$$

$$
\begin{aligned}
N_4(t) = N_4(0)e^{-\lambda_4 t} &+ \frac{\lambda_3\lambda_2\lambda_1 N_1(0)}{(\lambda_2-\lambda_1)(\lambda_3-\lambda_1)}\left(\frac{e^{-\lambda_1 t}-e^{-\lambda_4 t}}{(\lambda_4-\lambda_1)} - \frac{e^{-\lambda_3 t}-e^{-\lambda_4 t}}{(\lambda_4-\lambda_3)}\right) \\
&- \frac{\lambda_3\lambda_2\lambda_1 N_1(0)}{(\lambda_2-\lambda_1)(\lambda_3-\lambda_2)}\left(\frac{e^{-\lambda_2 t}-e^{-\lambda_4 t}}{(\lambda_4-\lambda_2)} - \frac{e^{-\lambda_3 t}-e^{-\lambda_4 t}}{(\lambda_4-\lambda_3)}\right) \\
&+ \frac{\lambda_3\lambda_2 N_2(0)}{(\lambda_3-\lambda_2)}\left(\frac{e^{-\lambda_2 t}-e^{-\lambda_4 t}}{(\lambda_4-\lambda_2)} - \frac{e^{-\lambda_3 t}-e^{-\lambda_4 t}}{(\lambda_4-\lambda_3)}\right) \\
&+ \frac{\lambda_3 N_3(0)}{(\lambda_4-\lambda_3)}\left(e^{-\lambda_3 t}-e^{-\lambda_4 t}\right).
\end{aligned}
\tag{2.24}
$$

Radon concentrations in water will be determined by using a radon-monitoring detector. According to S. Lorenz (F50/51 Limnophysics, 2011, pages 27 – 28), "the detector is not able to measure the radon activity concentration directly, but can measure the decay products of radon. Therefore, the relationship between radon and polonium in this section can be derived" [30]. The radioactive daughters of radon follow a decay chain starting with isotope ^{218}Po and progress to ^{214}Pb, ^{214}Bi and ^{214}Po, which decays into the long-lived ^{210}Pb and effectively ends the chain. The rates of change of the isotopes in the chain are described by the differential equations 2.15 to 2.18. The derived equations can easily show the relationship between radon and polonium in Equations 2.21 to 2.24.

After multiplying these concentrations by decay constants and dividing by ^{222}Rn activity at time t, the relative activities for each decay product are obtained. Based on these calculations, a build-up of ^{222}Rn progeny relative activities can be seen after around 200 minutes as the activities of the daughters reach the parent's activity [45].

2.3.4 Secular Equilibrium

In a decay chain, a condition called *secular equilibrium* may occur where the activities of the parent nucleus (P) and that of the short-lived daughter (D) are equal. The secular equilibrium underpins most of the nuclear techniques used for

measuring parent radionuclides indirectly through their progeny. The activity of the parent nucleus has a half-life much bigger than that of its daughter nucleus (i.e. $\lambda_P << \lambda_D$). We infer that after a time t the equilibrium state is reached and that the activity of the daughter nucleus is nearly constant [30].

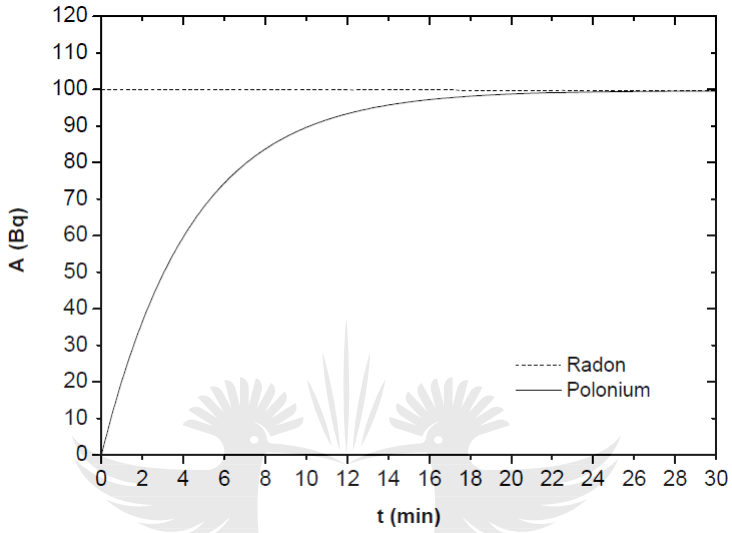

Figure 2.4: Secular equilibrium between the activity A of ^{222}Rn and ^{218}Po as a function of the elapsed time [30].

In S. Lorenz (F50/51 Limnophysics, 2011, pages 27 – 28), "the equilibrium state can be explained mathematically by the different half-lives [30]. After a period of time t, which is much longer than the half-life of the daughter, the term $e^{-\lambda_D t}$ is almost zero [30]. With this approximation and the activity of the parent nucleus $A_P(t) = A_D^0 \cdot e^{-\lambda_P t}$ the secular equilibrium is derived mathematically" [30]:

$$A_P(t) \approx A_D(t). \tag{2.25}$$

In the current study, ^{222}Rn in water has been determined by measuring the $\alpha-$ radiation associated with its progeny ^{218}Po and ^{214}Po. In the current study, the half-life of ^{222}Rn is much bigger than that of ^{218}Po. Therefore, the decay constant of radon is much smaller than the decay constant of polonium ($\lambda_{^{222}Rn} << \lambda_{^{218}Po}$) [31]. The secular equilibrium between ^{222}Rn and ^{218}Po is reached after 20 minutes whilst 3 hours between ^{222}Rn and ^{214}Po, as shown in Figure 2.4. In the current

study, the equilibrium between ^{222}Rn and its decay products will be the key to determine the radon activity concentration in water [11].

2.4 Radon Properties

2.4.1 General Properties

Radon is a naturally occurring noble gas, i.e., it is almost chemically inert and is not prone to combine with other atoms to create molecules. Radon has no colour, odor or taste and is therefore not detectable by human senses alone [9]. It is soluble in water, and its solubility decreases with increasing temperature [79]. Rodon has a density of 9.73 g.l^{-1} under standard conditions, which makes it to be it the heaviest gas in nature [40]. When cooled below its freezing point, radon has a brilliant phosphorescence which becomes yellow at lower temperatures (yellow $<$ -71.0 °C) and orange-red at the temperature of liquid air (-71.0 $<$ orange-red $<$ -61.8 °C) [42]. Upon condensation, radon glows because of the intense radiation it produces [2].

Radon is also referred to as a metalloidelement which lies on a diagonal between the true metals and nonmetals in the periodic table. It has some of the characteristics of both groups behaving similarly to boron, germanium, antimony and polonium [44]. Some physical properties of radon are given in Table 2.2. From L. Tommasino (Radiochemical methods, 2015), "radon is absorbed in charcoal, silica-gel and similar substances. This allows to separate it from other gases. Radon can be effectively removed from a sample air stream by collecting it on activated charcoal, cooled to the temperature of solid CO_2 ($-78.5\,^{\circ}$C)" [25]. Radon is desorbed from charcoal by heating it up to 350 °C [40].

Radon is the element with atomic number 86 in the periodic table. The electrons completely fill the outer shell of radon so there are no free electrons. The stability of the electronic configuration ensures that radon does not react with other elements under normal conditions. All types of soil contain naturally occurring primordial radionuclides such as ^{238}U, ^{232}Th and ^{40}K. These radionuclides have

Table 2.2: Properties of radon (^{222}Rn) [39].

Parameters	Property
Relative Atomic Mass	222.02
Boiling Point	$-61.8\,^{\circ}$C
Melting Point	$-71.0\,^{\circ}$C
Density	9.96 kg m^{-3}
Molar Volume	50.5 cm^3 mol^{-1}
Physical State at 20 $^{\circ}$C	Gas
Half-life ($T_{1/2}$)	3.825 days
Electron Configuration	[Xe] 4f^{14}5d^{10}6s^{2}6p^6

long half-lives and were present from the time of earth's formation, thus radioactivity has always been part of life. Within the ^{238}U decay series (Figure 2.1a), radon is produced by the decay of ^{226}Ra, which occurs in minute quantities in the rocks and soil [42].

Studies of radon in water complement the use of long-lived isotopes such as ^{3}H and ^{14}C with half-lives of 12.43 and 7 530 years, respectively. These isotopes have been used to measure the hydrological cycle of groundwater from months to thousands of years. The consumption of water with elevated amounts of radon pose a radiological hazard to the public using private wells [43]. In the uranium-238 series shown in Figure 2.1a, the radiation is emitted in the form of alpha, beta particles, and gamma photons ($\alpha-, \beta-$particles and $\gamma-$photons). These emissions are the basis through which radioactivity is measured by the radiation detectors.

2.4.2 Physical Properties of Waterborne Radon

Siddig (PhD 2009, pages 24 – 26), "radon is colorless, odorless, tasteless, chemically inert and radioactive. During the radioactive decay process, radon can move from its point of origin and dissolves in groundwater. Because of its gaseous nature, radon can easily escape when the water containing radon is exposed to the air which makes its concentration low in surface water or rivers. gas is mildly soluble in water, but, being a gas, is volatile" [53]. It tends to leave the water upon contact

with air. This is known as aeration [67]. The rate of radon transfer from water to air increases with sample temperature, agitation, mixing, and surface area [46]. Sylvia Lorenz cited in S. Lorenz (F50/51 Limnophysics, 2011, pages 31 – 32), "in principle, the radon will continue to be released from water as the aeration process continues, until a state of equilibrium develops. According to Henry's Law of dilute solutions, equilibrium will occur when the water and air concentration reach a fixed ratio for a certain temperature [30]. This ratio, derivable from Henry's Law constant for radon dissolved in water, is known as the distribution or partition coefficient ($k_{w/a}$)" [53].

As noted by Siddig (PhD 2009, pages 24 – 26), "for radon in water at 20 °C the $k_{w/a}$ value is about 0.25, so radon will continue to be released from the water until the water concentration drops to about 25 percent of the air concentration [53]. Remember that as the radon leaves the water into the air it raises the air concentration and lowers the water concentration [53]. At lower temperatures the distribution coefficient increases, rising to 0.51 at 0 °C [53]. At higher temperatures the distribution coefficient decreases, dropping to about 0.11 at 100 °C as shown in Table 2.3" [53].

Table 2.3: Partition coefficient of ^{222}Rn between water and air [56].

T (°C)	$k_{w/a}$	T (°C)	$k_{w/a}$
0	0.51	50	0.14
5	0.42	55	0.13
10	0.35	60	0.12
15	0.30	65	0.12
20	0.25	70	0.12
25	0.22	75	0.11
30	0.19	80	0.11
35	0.17	85	0.11
40	0.16	90	0.11
45	0.15	95	0.11

The distribution of radon in the pores between water and air phases depends on the water temperature and the atmospheric partial pressure of radon. When radon

concentration reaches equilibrium between water and air, the partition coefficient decreases exponentially with increased temperature as shown in Figure 2.5 [94]. Because of this partitioning, radon in water has been determined by measuring radon in air degassed from the water in question [14]. Table 2.3 shows values of the partition coefficient at various temperatures, taken from two references. The partition coefficient dependence on temperature T (in °C) has also been parameterized by the relation [55]:

$$k_{w/a}(T) = 0.105 + 0.405e^{-0.0502T}. \tag{2.26}$$

Radioactivity in soil is related to radioactivity in rocks from which the soil is formed. Since uranium and radium can be found throughout the earth's crust and radium is also soluble in water, radon is found virtually everywhere [41].

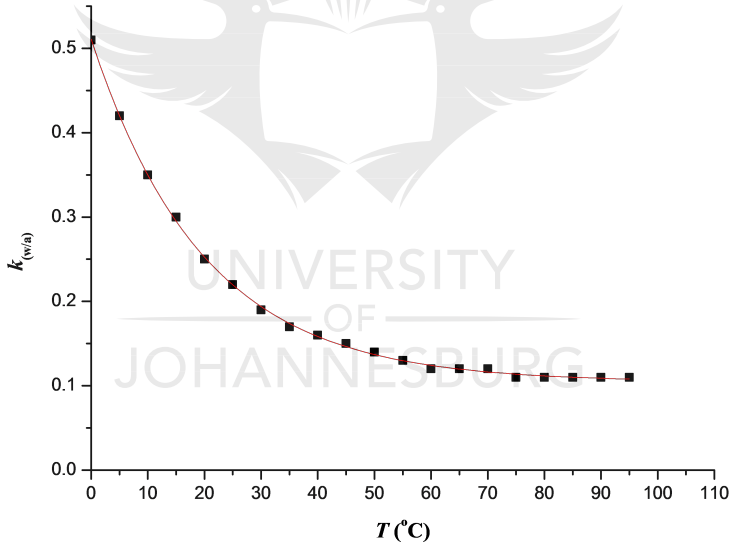

Figure 2.5: Partition coefficient between water and air, $(k_{w/a})$ as a function of temperature.

2.5 Radon Genesis

Naturally occurring radon originates from radium that is present in soil or rock. ^{222}Rn is a progeny of ^{226}Ra, which is characterized by the level of ^{238}U in soil

[83]. This way, the rate of radon production in soil is influenced by the distribution of uranium in the earth's upper crust. The average concentration of uranium and thorium in the top 0.3 meter of soil is 1 ton and 3 tons respectively, per square mile [83].

A ^{226}Ra atom, residing in a mineral grain, decays by ejecting an $\alpha-$particle (^{4}He) and forms a ^{222}Rn atom that recoils in a direction opposite to that of the $\alpha-$particle. By this recoil process, the ^{222}Rn atom may be released (emanate) from the mineral grains [53]. This process is called direct recoil emanation which is the dominant radon emanation process. Depending on the grain density, the direction of recoil and the location of the ^{226}Ra atom in the grain, the radon atom moves a distance of 0.02 – 0.07 μm and could possibly land in a pore space [52].

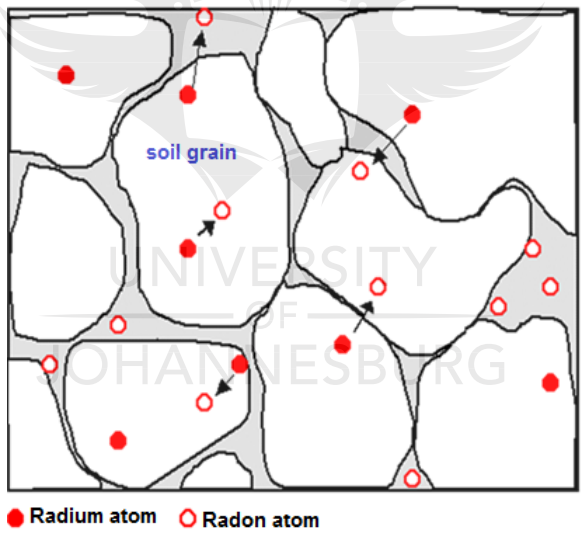

Figure 2.6: Schematic drawing of a suite of mineral grains illustrating various scenarios following radon generation [53].

Radium atoms decay to radon and the radon atoms are dislodged from the grain by the recoil process. Figure 2.6 illustrates how some radon atoms have been able to emanate from the grains [53]. The emanation occurs when radon atoms recoil in a direction towards adjacent air pores or water-filled pores. If the pore space is filled with air, the radon atom may cross the pore space and get embedded and

immobilized in an adjacent grain. The range of the recoil radon atom in water is less compared to its range in air, therefore, the radon atom may end up in water and hence the emanation rate increases with increasing pore water [53].

Radon concentrations in air pores or in water filled pores are determined by the number of radon atoms emanated into the pore space, the porosity, and the water content of the soil. In addition, these radon concentrations decrease because some of the radon atoms are moved away from the source either with the airborne soil or with the flowing water. Under conditions of no ventilation, the radon concentration in a soil's pores filled with air or water, C_{max} (Bq.m^{-3}), is given by [52]:

$$C_{max} = AED\left(\frac{1-p}{p}\right), \tag{2.27}$$

where A is the specific activity (Bq.kg^{-1}) of ^{226}Ra in the soil, E is the emanation coefficient (the ratio of the total amount of radon that emanate to the pore space to the radon produced in the mineral grains, D is the compact density (normal for mineral soils = 2 700 kg.m^{-3}) and p is the porosity. C_{max} is sometimes called equilibrium concentration where the radon concentration in water is in secular equilibrium with the emanation from the aquifer rocks. The emanation rate is generally varied with the grain size. For example, radon emanation is higher for fine clay than it is for sand [53].

2.6 Radiation and Health

The health detriment caused by ionizing radiation is based on the energy imparted to a tissue, for instance by $\alpha-$ or $\beta-$particles, neutrons or photons. This energy can induce chemical reactions in the tissues, such as DNA breakage or the formation of free radicals that can further damage DNA strands. If the cells are not able to repair DNA damage properly, early senescence, apoptosis or mutations occur, the latter of which may lead to cancer [57]. As $\alpha-$particles have the highest mass and energy, they release their energy in a very short distance (tens of micrometres),

and hence incur more local damage to tissues than $\beta-$particles or $\gamma-$photons [48].

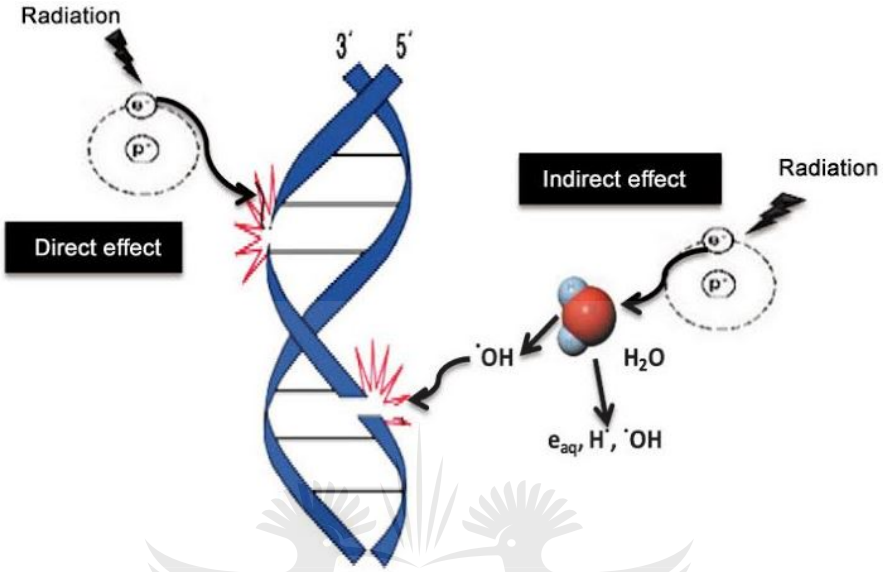

Figure 2.7: Representation of the direct and indirect effect of ionizing radiation on DNA [57].

The hazard caused by radiation is governed by several factors such as the radiation type, energy and activity, the transfer of a radioactive element inside the body, the biological half-life, physical half-life and target tissue [48]. The quantity in assessing doses from radiation is the absorbed dose, D, which is the energy imparted per unit of mass. Its unit is the gray (Gy), which equals J.kg^{-1} [48]. The equivalent dose, H_T, is defined as the average absorbed dose in a volume of a specified organ or tissue due to radiation of type R [48]:

$$H_T = \sum_R w_R D_{T,R}, \tag{2.28}$$

where w_R is the radiation weighting factor [48]. The radiation weighting factor reflects the harmfulness of the radiation type [48]. For photons ($\gamma-$rays) and $\beta-$particles it is 1 and for $\alpha-$particles 20. The unit of the equivalent dose is the sievert (Sv). It must be noted that the equivalent dose is always specific for a tissue

or an organ [51]. The effective dose, E, is defined by the weighted sum of tissue or organ equivalent doses [51]:

$$E = \sum_T w_T H_T, \tag{2.29}$$

where w_T is the tissue weighting factor [51]. The unit of the effective dose is also the sievert (Sv) [51]. The tissue-weighting factor has been defined as 0.12 each for bone marrow, the colon, lungs, stomach, breasts and the remaining tissues. For the gonads, the weighting factor is 0.08, and for the bladder, oesophagus, liver and thyroid it is 0.04 [51]. For the bone surface, brain, salivary glands and skin it is 0.01 [51]. Considering the linkage between the cancer risk and effective dose, the International Commission on Radiological Protection (ICRP) has assessed the detriment-adjusted cancer risk to be 5.5×10^{-2} Sv^{-1} for the whole population and 4.1×10^{-2} Sv^{-1} for adult workers [51]. This means that if a person is exposed to an effective dose of one sievert, his or her cancer risk increases by 5.5 percentage points over a long period of time [31]. The dose-response relationship is hence thought to be linear [51].

The effective dose can also be understood as a quantity of projected risk. It must be noted that dosimetric risk assessments may hold large uncertainties because the risk is extrapolated from high exposure situations and it may not therefore be representative for a low exposure range [29]. Epidemiological data on the dose-response relationship in this range are generally lacking. However, evidence supporting a linear dose-response relationship exists for inhaled radon, although evidence is still absent for ingested radon [29].

2.6.1 Radon in Surface Water

R. Engelbrecht (Handbook of Radioactivity Analysis, Third Edition, pages 695 – 726, 2012) elaborated on about the surface water and indicated that, “Surface water comprises rivers, lakes, or seawater, and is one of the environmental components to which radioactive effluents from nuclear installations are authorized

to be discharged [91]. Radionuclides in surface water can be found in the water phase or associated with suspended particles and can eventually become incorporated into sediments and living species [91]. Natural radionuclides in river water include ^{3}H at levels of 0.02 – 0.1 Bq.l^{-1}, ^{40}K at 0.04 – 2 Bq.l^{-1}, radium, radon, and their short-lived decay products at $<$0.4 – 2 Bq.l^{-1}. The main fraction of ^{3}H in surface water however is due to anthropogenic activities" [91].

R. Engelbrecht (Handbook of Radioactivity Analysis, Third Edition, pages 695 – 726, 2012) "Some of the sampling methods are automatic and continuous and designed to give an early warning in case of an accidental release. In all cases, additional information on the river flow rate is very important. Samples can be taken continuously and are then bulked onto monthly or quarterly analysis, or alternatively spot samples are taken periodically and analyzed individually. The time and frequency information can be analyzed for seasonal hydrological variations. Treatment of water may consist of filtration, the filtered water and suspended material being measured separately, ion exchange and subsequent washing of the ion-exchange column, or evaporations (for direct measurement of the residue)" [27].

2.6.2 Measurement Techniques and Methods

Radon cannot be detected by human senses, but nuclear signatures that come from $\alpha-$ and $\gamma-$ radiation, produced by radon and its progeny, are the main key for measuring its presence. Generally, according to Richard Cothern and James Smith Jr (Environmental Radon, 1987, pages 77 – 79) "measurement techniques can be divided into three categories: grab sampling, continuous and active sampling, and integrative sampling [54]. The main reasons for choosing between these categories are costs, time, type of information required, and desired accuracy".

The *Grab* sampling technique implies a short sampling time (a few minutes). It is useful for indoor radon measurements, as it provides a quick screening of a residence to determine if there is an extremely high radon concentration [54]. Radon grab sampling is based on a very slow drawing of a small air volume into

the counter chamber through a millipore filter. During the filtering, most of the airborne radioactive particulates are removed, including radon progeny that are attached to dust and aerosols. When radon decays in the chamber, it produces daughters, and the alpha particles, emitted in the decay of radon and its progeny, are counted by an alpha scintillation counter or an ionization chamber [54].

The *Continuous* sampling technique is based on automatic measurements that are taken at closely spaced time intervals over a long period of time [79]. This results in a series of measurements which can supply information on how the concentration varied during the experiment [54]. An example of continuous radon measurements is shown by Kavasi *et al.* [54] as a function of time in the tunnel of a Hungarian manganese mine.

2.7 Detection System

In the contribution by N. Vajda, P. Martin and C-K. Kim (Handbook of Radioactivity Analysis, pages 363 – 422, 2012), the detection system was presented in the following manner, "The core part of an $\alpha-$spectrometer is the detector, where the interaction of the particle with the matter of the detector takes place [69]. The energy of the alpha particle is transformed to a measurable physical quantity, e.g. electric charge, current, or voltage. In the process of detection, the charge carriers are collected and converted to electric pulses. In spectrometry, pulse are processed in the *'pulse mode'* where each interacting particle is detected independently [69]. Electric pulse processing units such as preamplifiers and amplifiers attached to the detector output, both amplify and form (shape) the pulse. Pulses are then digitized by an analog-to-digital converter (ADC). From a series of digitalized pulses of different heights at the ADC output, the multichannel analyzer (MCA) generates a pulse-height spectrum by sorting the pulses according to their heights and assigning them to a channel number proportional to the pulse height" [27].

An alpha spectrometer schematic diagram as presented by N. Vajda, P. Martin and C-K. Kim (Handbook of Radioactivity Analysis, pages 363 – 422, 2012), is

shown in, "Figure 2.8 [27]. Alpha spectrometers may contain vacuum chambers surrounding the detector and the source [27]. Vacuum supply units usually contain vacuum pumps such as oil rotation pumps, vacuum gauge, and occasionally a vacuum control system to adjust the desired pressure [27]. In a spectrometric application, the basic information of the radiation (i.e. the type of radiation, the energy of the particles, and the activity of the source) is conserved in the form of the shape and height of the electric pulses, and the pulse frequency or count rate" [27].

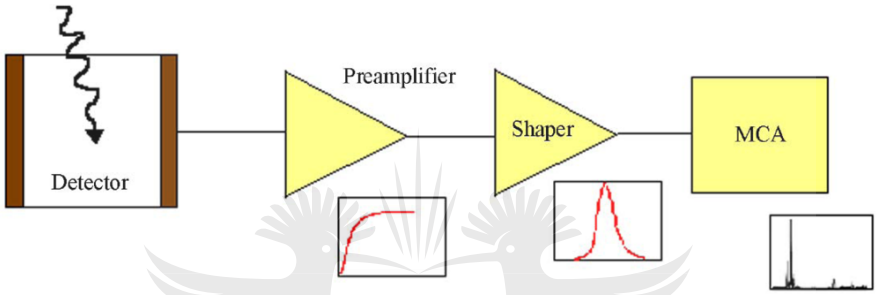

Figure 2.8: Figure showing an $\alpha-$spectrometer diagram [27].

2.7.1 *Interaction of $\alpha-$radiation with the Materials of the Detector*

In order to understand how to maximise the functionality of the detector, it is also important to understand the behavior of the $\alpha-$radiation when it interacts with the detector material. Hence, N. Vajda, P. Martin and C-K. Kim (Handbook of Radioactivity Analysis, pages 363 – 422, 2012) noticed that, "only a few radiation detector types are suitable for the accurate determination of the energy distribution of alpha particles. Of these, silicon semiconductor detectors are the most frequently used at present [69]. Due to instrumental improvement and developments in spectrum evaluation software, high-resolution alpha spectrometry using Si detectors became available from the end of the 1980s [69]. Among gas ionization detectors, ionization chambers and proportional counters have been used in alpha spectrometry and a special type of gas detector has been developed for the determination of pulse-height distribution of alpha particles, the gridded ionization chamber [69]. Although scintillation detectors have in general relatively poor

energy resolution, the development of a *high-resolution* alpha-liquid-scintillation spectrometer in combination with selective chemical procedures offers some advantages in alpha spectrometry" [27].

It was further outlined by N. Vajda, P. Martin and C-K. Kim (Handbook of Radioactivity Analysis, pages 363 – 422, 2012), "the process of detection of alpha particles by various nuclear detectors is determined by the interactions between the particle and the detector [27]. When alpha particles enter the detector, they immediately interact with the atomic electrons of the detector material [27]. The main results of this interaction are excitation and ionization. In the latter case, an electron and positron ion (cation/hole) pair formed [27]. Along its path through the detector the high-energy alpha particle will create a large number (N) of electron-cation pairs [27]. N can be expressed as"

$$N = \frac{E_\alpha}{\varepsilon}, \tag{2.30}$$

where the variables of the equation were defined by N. Vajda, P. Martin and C-K. Kim (Handbook of Radioactivity Analysis, pages 363 – 422, 2012), "E_α is the energy of the alpha particle and ε is the energy needed to form one electron-cation pair. Since E_α is in the range of a few MeV and ε is depending on the type of detector - in the range of 1 eV to 100 eV, a single alpha particle can produce 10 000 to 1 000 000 charge carriers while it loses its energy before it is stopped. The track of the alpha particles in the detector is almost straight because the heavy particles are not significantly deflected by the interacting electrons. The specific energy loss of the alpha particle, also called the stopping power, is described by the Bethe formula" [27]. *Wikipedia: The free encyclopedia* (2017, January 17), "for a particle with speed v, charge z and energy E, traveling distance x into a target of electron number density n and mean excitation potential I, the relativistic version of the formula reads, in SI units" [50]

$$-\langle\frac{dE}{dx}\rangle = \frac{4\pi}{m_e c^2}\cdot\frac{nz^2}{\beta^2}\left(\frac{e^2}{4\pi\varepsilon_0}\right)^2\cdot\left[\ln\left(\frac{2m_e c^2\beta^2}{I\cdot(1-\beta^2)}\right)-\beta^2\right], \tag{2.31}$$

where c is the speed of light, ε_0 the vacuum permitivity, e and m_e the electron charge and rest mass respectively [59, 60] for experimental determination of I for various elements and thorough treatment of stopping power calculations. N. Vajda, P. Martin and C-K. Kim (Handbook of Radioactivity Analysis, pages 363 – 422, 2012) further illustrated that, "the $\alpha-$particle interaction with the detector is characterized by a range or distance beyond which no particles penetrate. This range depends on the energy of the alpha particle and the type of detector, i.e. its atomic number and density [27]. As an example, the range of alpha particles in Si is shown as a function of alpha energy in Figure 2.9" [27].

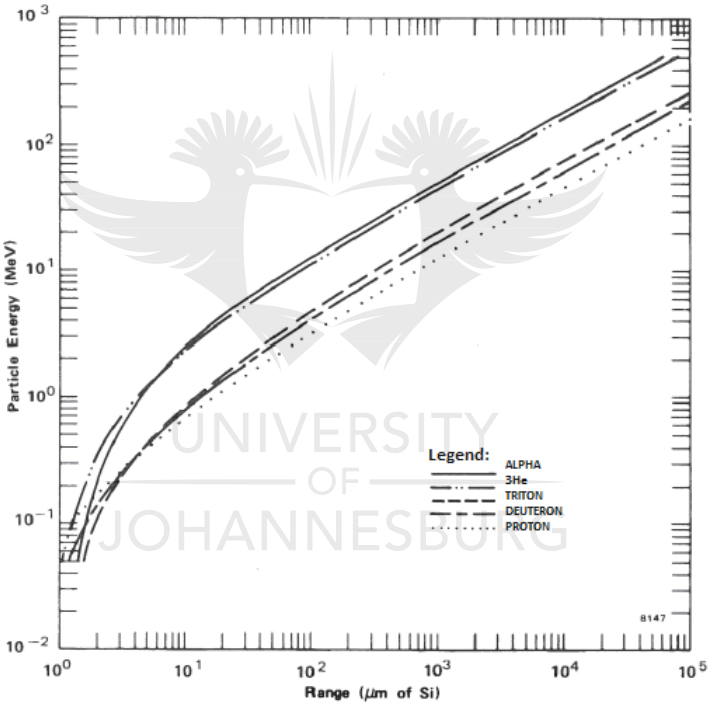

Figure 2.9: The graphic representation of the range of alpha particles in silicon [27].

N. Vajda, P. Martin and C-K. Kim (Handbook of Radioactivity Analysis, pages 363 – 422, 2012), "since alpha energies of radionuclides are not higher than 10 MeV, they are completely absorbed in Si layers of 100-μm thickness [69]. Thus, Si detectors should not be significantly thicker if they are used for the measurement of alpha-emitting radionuclides [69]. In the case of gas detectors, the de-

tector thickness depends on the type and especially on the pressure of the gas in the detector chamber [69]. Around atmospheric pressure, the range of 10 MeV alpha particles is about 5 – 10 cm, and so this is the desired detector size [69]. The very short range of alpha radiation enables the design of detectors, which are able to completely absorb the incident radiation, without requiring large detector volumes [69]. This fact, combined with the large number of charge carriers that are produced, is responsible for the higher counting efficiency that is typical of alpha spectrometry" [27].

N. Vajda, P. Martin and C-K. Kim (Handbook of Radioactivity Analysis, pages 363 – 422, 2012), "however, the limited range of alpha radiation is also responsible for the major challenge in alpha particle detection, which is ensuring that alpha particles reach the active volume of the detector without significant losses [69]. This means the reduction or elimination of absorption in the source, any absorbent layers between source and detector, and in the detector window [69]. Absorption and self-absorption in the detection process can be reduced by ensuring direct contact between the source and the detector, e.g., by placing the source inside the detector gas chamber or by dissolving the source in a liquid detector, as in the case of liquid scintillation counting (LSC) [69]. In the case of silicon detectors, absorption can be reduced by the use of a vacuum in the chamber surrounding the detector and the alpha source" [27].

2.7.2 Semiconductor Silicon Detectors

N. Vajda, P. Martin and C-K. Kim (Handbook of Radioactivity Analysis, pages 363 – 422, 2012), "semiconductor Silicon (Si) detectors are regarded as analogous to gas ionization as solid-state ionization detectors [69]. The use of a solid medium has the advantage that the dimensions of the detector can be kept small while the counting efficiency is as high as in case of gases [69]. In $\alpha-$spectrometry, this means that a 100 % intrinsic efficiency can be reached with a Si detector of $100-\mu m$ thickness [69]. A major advantage of semiconductors is their high-energy resolution [69]. A drawback includes the limitations on size and their high susceptibility to radiation-induced damage resulting in spectrum degradation

[69]. There are some differences in the pulse generation processes between gas ionization and semiconductor detectors, which are as follow [27]:

- The mobility of the charge carriers is different. In gas ionization detectors, the mobilities of the electrons are about 1 000 times higher than those of the cations, while in semiconductor detectors, the mobilities of the electrons are 2 - times higher than those of the holes;

- The charge collection times are different. The time needed to collect – cation pairs is in the range of μs; and

- The size of the sensitive volume is dependent on the applied voltage in semiconductor detectors, while it is constant in gas ionization detectors."

N. Vajda, P. Martin and C-K. Kim (Handbook of Radioactivity Analysis, pages 363 – 422, 2012) further noted that, "the properties of semiconductor materials including the description of the structure have been discussed in detail in many good monographs [61]. In Si semiconductor detectors, p-type and n-type Si are brought together in good contact, and a reverse bias (positive to the n-type Si) is applied. At the junction of two Si layers, an intrinsic layer depleted in any charge carrier is formed. The reverse-biased p-n diode, is used as an $\alpha-$particle detector [61]. The basic interaction between the ionizing particle and the detector takes place in the depleted/intrinsic region. When the alpha particle passes through a semiconductor, electron-hole pairs are created along the track [61]. These charge carriers are collected by the electric field, which changes in the electric field being registered as pulses [69]. Pulse amplitudes are small, being in the range of μA. Since the height of the pulse is proportional to the energy deposited by the interacting particle, the detector is suitable for spectrometric measurements" [27].

According to fabrication technology, N. Vajda, P. Martin and C-K. Kim (Handbook of Radioactivity Analysis, pages 363 – 422, 2012) noted that, "silicon semiconductor detectors are of three different types: the diffused junction detectors (DJD), the surface barrier detector (SBD), and the passivated ion-implanted detector (PIPSi) [69]. Each detector can be regarded as a reversed-biased compen-

sated detector where n- and p-type Si crystals are brought into contact and a depleted/intrinsic (i) layer is formed as the sensitive volume of the detector" [27].

Major characteristics of Si semiconductor detectors are as follow [27] as per N. Vajda, P. Martin and C-K. Kim (Handbook of Radioactivity Analysis, pages 363 – 422, 2012):

- "Surface barrier and preferably passivated implanted planar Si detectors are used to obtain alpha spectra;
- Pulse amplitudes are usually very small (in the range of a few μA) but well detectable after amplification;
- The typical leakage current of a PIPSi detector is in the range of nA;
- Energy resolution of the detector is high due to the low ionization energy needed to create an electron-hole pair. Typical resolution of the detector is 10 to 20 keV depending on detector performance and size;
- Charge collection times for electron-hole pairs are fast, in the range of μs. There is a relatively small difference between the collection times of electrons and holes (a factor of 2 to 3);
- Absolute counting efficiencies are close to 50% if sources are placed close to the detector inside the chamber; and
- Si detectors usually have low background resulting in a high counting sensitivity".

2.7.3 Scintillation Detectors

N. Vajda, P. Martin and C-K. Kim (Handbook of Radioactivity Analysis, pages 363 – 422, 2012), "detection of ionizing radiation by scintillation detectors is based on the emission of light as a result of the interaction of the radiation with the detector material (called a scintillator) followed by the collection of light and

its conversion into electrical pulses using photomultiplier tubes (PMTs) or photodiodes. Scintillation detection is one of the oldest techniques in the measurement of radioactivity having had widespread application for the detection of $\alpha-, \beta-$, and $\gamma-$ radiation in the past [69]. At present, most of the applications are related to gross counting of alpha, beta, and gamma radiation due to typical high counting efficiency and the low cost of the instrumentation while radiation spectroscopy is limited by the insufficient energy resolution of the scintillators to allow the identification of the radionuclides in an isotope mixture. Scintillation $\gamma-$spectrometry was a basic tool until the 1980s, but it was gradually replaced by semiconductor spectrometry of much better energy resolution" [27].

N. Vajda, P. Martin and C-K. Kim (Handbook of Radioactivity Analysis, pages 363 – 422, 2012), "the main parts of a scintillation detector are the scintillator, which converts the radiation energy to visible light photons, and the photoelectron-multipier (PM) tube containing the photocathode, the multistage electron-multiplying section made of a series of electron-multiplying dinodes and an anode for collection of the amplified charge situated in a glass vacuum envelope [69]. Photocathodes are responsible for converting the energy of the photons into electrons. If the light appears as a pulse, the photoelectrons produced will also form a pulse in the similar time duration [69]. The number of electrons emitted by the cathode is multiplied on the dinodes where the multiplication factor can be as high as $10^6 - 10^8$ depending on the applied voltage [69]. The electric pulse at the anode of the PM tube can be directly counted without further amplification by a simple counter, a single or a multichannel analyzer [69]. Typical tubes have fast response times. When they are illuminated by a short light pulse, an electron pulse will be produced at the anode with a time width of a few nanoseconds after a delay time of 20 – 50 ns "[27].

2.7.4 *Detection of $\alpha-$particles by LSC*

N. Vajda, P. Martin and C-K. Kim (Handbook of Radioactivity Analysis, pages 363 – 422, 2012), "Liquid scintillators are frequently used for the detection of $\alpha-$particles [69]. Commercial liquid scintillation counters (LSCs) developed for the detection of low-energy $\beta-$particles can be used to measure $\alpha-$particles with-

out self-absorption losses, giving 100 % absolute counting efficiency [69]. This advantage is counterbalanced by the limited resolution of the scintillators [69]. A typical energy resolution using a commercial LS system is about 20 to 25 %; so $\alpha-$spectrometry is difficult or almost impossible to achieve [69]. Detection of low-level alpha radiation by commercial LSC is difficult because the scintillation yield of the $\alpha-$particles is lower by about a factor of 10 than that of $\beta-$particles. Therefore, the spectra of the alpha radiation of 4 to 6 MeV appear in the same region as the spectra of $\beta-$particles of 400 to 600 keV" [27].

3 Experimental Methods

3.1 Detection and Measurement of Radon in Water

In the current study, radon concentration in was measured in the river water using an $\alpha-$spectrometry technique. For the proper functionality of the equipment, a number of different meteorological parameters have been tested. Radon concentration in the water can be measured on site or can be collected from the site to the laboratory. Because of its nature which is an inert gas, radon dissolves in water, but does not react with water.

Radon-in-water can either be measured in the laboratory after collecting the samples, taking into account the decay correction or measured in-field [9]. Sampling and transportation require extra care to reduce radon loss before analysis. Measurement of radon concentration from the rivers in the Gauteng Province was carried out by counting $\alpha-$particles emitted by the progeny of radon, ^{218}Po and ^{214}Po [9]. During the collection and transportation of the water samples from the rivers to the laboratory, a special attention on the type of sample holder equipment and the sample storage taken considered to minimize radon loss before the experiment could be conducted [33].

Laina Salonen further noted in Chapter 9 (Handbook of Radioactivity Analysis (Third Edition, pages 625 – 693)), “To avoid some of the radon being lost by adsorption onto the surface of polyethylene, glass bottles are normally been used [64]. The caps were equipped with a rubber or Teflon septum to prevent radon leakage from the bottle. Sampling instructions depend on the sampling situation and purpose” [33]. In the current research, a bubbler method which used an

$\alpha-$spectrometry with low background and low detection limit, which is about 50 Bq.m^{-3} was deployed [39].

3.2 The Detector of Choice

3.2.1 Alpha-spectrometry using Solid-state Alpha Detectors

According to N. Vajda, P. Martin and C. Kim, the $\alpha-$spectrometry "is a widely applied radioanalytical technique, primarily due to its high counting efficiency and low intrinsic background, its versatility in terms of both the range of radionuclide and sample types which can be analyzed and the reliability of the technique due to the possibility to use an $\alpha-$emitting isotope of the element of interest as an internal tracer" [69].

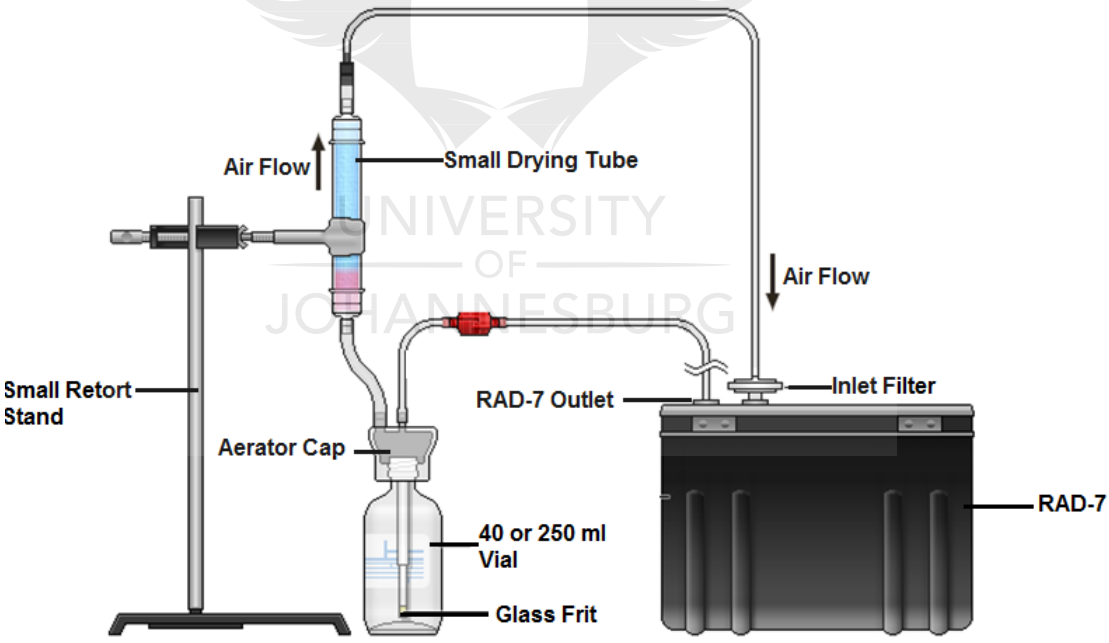

Figure 3.1: Schematic representation of the experimental setup using a grab sample and a radon-in-air monitor, an $\alpha-$spectrometry method [67].

Figure 3.1 represents an experimental set-up using a grab sample and a radon-in-air monitor [71], which uses well defined signals in a solid-state alpha detector as a continuous radon monitor. The monitor applies the $\alpha-$spectrometry process. It is a highly versatile instrument, used to measure radon in real-time and designed to detect $\alpha-$particles only [66]. The detector's major advantage is its high sensitivity, with detection limits as low as 1 mBq per sample being easily achievable. This arises due to several factors, N. Vajda, P. Martin and C-K. Kim (Chapter 6 of the Handbook of Radioactivity Analysis (2012), pages 363 – 422) [69] listed about five points as shown below:

- "The spectroscopy at high resolution for the alpha peaks which are highly specific indicators of the presence of radon;
- *high yield of the $\alpha-$decay process*. For most $\alpha-$emitting radionuclides, there are only a few peaks within a relatively small energy range, representing a total intensity of or close to 100 % of decay [69];
- *the built-in semiconductor alpha detector*, has a low intrinsic background being typically 10^{-5} and 10^{-6} cps [70]of an uncontaminated detector;
- *the intrinsic efficiency of the detector system* is close to 100 % for incident $\alpha-$particles [69]; and
- *low sensitivity of the semiconductor $\alpha-$ detector to $\beta-$ and $\gamma-$ radiation*" [69].

The interior of the RAD-7 instrument contains a hemisphere of 0.7 l volume with an ion-implanted silicon solid-state $\alpha-$ detector, and an air pump to be found at the centre. A representation of the measurement chamber with the detector is shown in Figure 3.2 [72].

The high voltage power circuit charges the inside conductor to a potential of 2 000 to 2 500 V, creating an electric field throughout the volume of the detector [73]. The radon in the air is sucked inside and it decays into the positive ions of $^{218}Po^{+}$

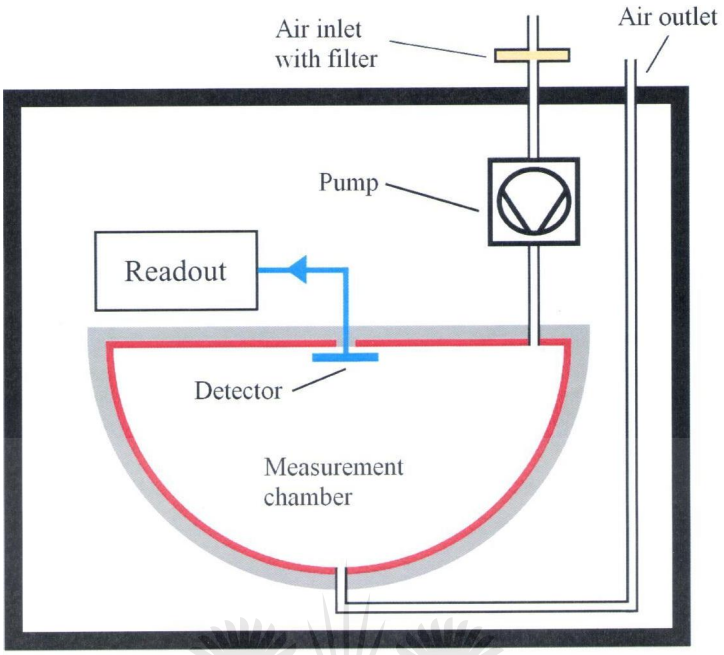

(a) The internal cell of the RAD-7.

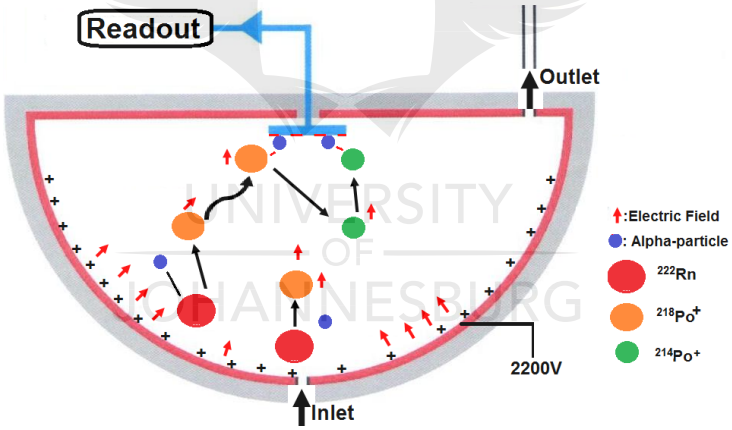

(b) Detection processes in the RAD-7.

Figure 3.2: The internal process of the measuring chamber of the RAD-7 detector.

($T_{1/2}$ = 3.05 min; α-energy = 6.00 MeV) and $^{214}Po^{+}$ ($T_{1/2}$ = 164 μs; α-energy = 7.67 MeV), which are attracted by the electric field and may be deposited on to the detector, which is at ground potential, before they are neutralized [79]. The emitted $\alpha-$particles of characteristic energy produce an electrical signal pulse.

The signal is amplified electronically and transformed into a digital signal and the energy of the signal is histogrammed by the microprocessor to form a spectrum [30]. The energy of the $\alpha-$particle is linearly proportional to the electrical pulse voltage [30].

One of the many advantages of using this detector is its ability to immediately differentiate between different radionuclides by their $\alpha-$energy using $\alpha-$spectroscopy (e.g. separate radon from thoron by the energy) [5]. The humidity inside the chamber must be kept low to prevent the ions from being neutralized so that the positive ion collection efficiency is high [5]. This explains the need for the desiccant, a laboratory-drying unit that is made of $CaSO_4$ granules, which have a high affinity for water, so it absorbs moisture before it reaches the RAD-7 detector chamber [5]. Normally the RAD-7 instrument operates well at a humidity of less than 10 % [14] and activity can be measured below 4 Bq.m^{-3}.

3.2.2 Measurement of Radon in water using a RAD-7 Detector

The RAD-7 detector uses the RAD-H_2O accessory which enables it to measure radon in water over a concentration range of less than 10 pCi.l^{-1} (0.37 Bq.l^{-1}) to greater than 400 000 pCi.l^{-1} (14 800 Bq.l^{-1}) [68] in a short time. It measures the activity of the sample giving results in about 30 minutes. This technique employs a closed-loop concept, consisting of four components, the RAD-7, tube desiccant, water vial aerator and connection tubes (see Figure 3.3) [8]. In this system, air is bubbled through a vial of either 40 ml or 250 ml with a water sample in five minutes, to release the radon gas from water. The ^{222}Rn diffusing from the water sample continuously circulates through a desiccant column then on to the RAD-7 detector, and then back to the water sample (vial) to establish equilibrium between the radon in the water and the air. The system waits for another five minutes, making it 10 minutes of bubbling, so that ^{218}Po and ^{222}Rn are ensured to be well in equilibrium. The final concentration of radon in the gas and the liquid phase can be described by Henry's law [30], which states that the mass of a gas which is dissolved into a solution is directly proportional to the partial pressure of that gas above the solution.

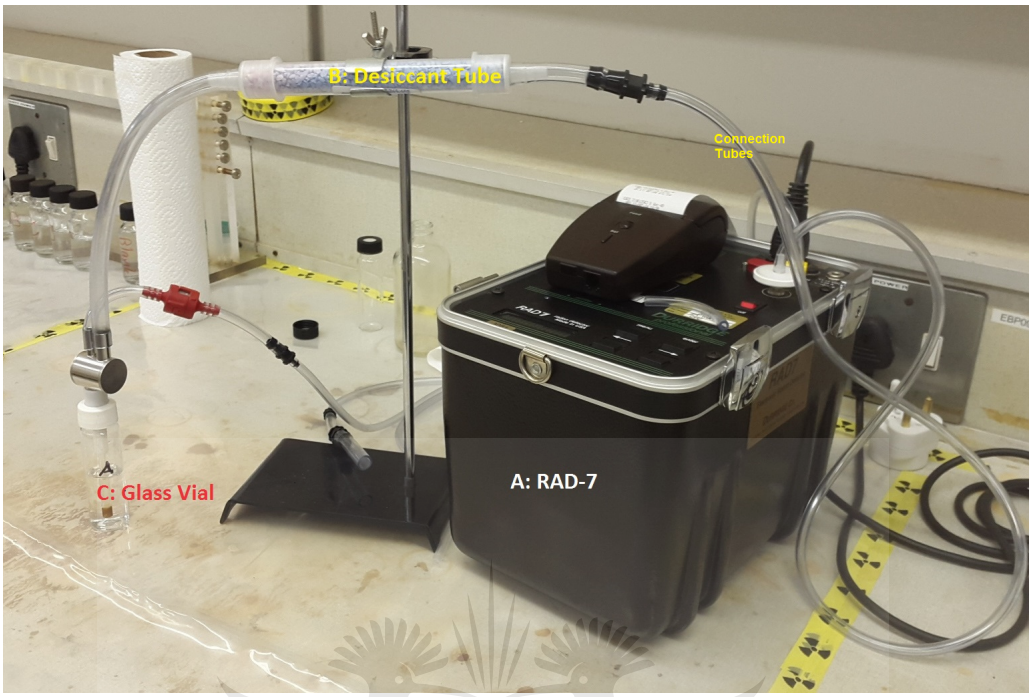

Figure 3.3: RAD-7 set-up at Necsa's Radio-Analysis Laboratory.

In the publication by I. Stojkovic, B. Tenjovic, J. Nikolov (Improvement of measuring methods and instrumentation concerning ^{222}Rn determination in drinking waters - RAD-7 and LSC technique comparison, 2015), "factors that affect the measurement accuracy and precision of the RAD-7 radon detector are the sampling technique, sample concentration, sample size, counting time, internal cell temperature, relative humidity (*RH*) and background effects [74]. *RH* showed the greatest impact on the measurement error in the presented results, since it reduces the efficiency of collection of the ^{218}Po atoms formed when radon decays inside the chamber [74]. For accurate readings, the RAD-7 instrument should be dried out thoroughly before making the measurement [74]. The *RH* inside the instrument should stay below 10 % for the entire 30 min of measurement. The most significant background effect in the RAD-H_2O are counted from radon daughters and traces of radon left from previous measurements, especially after a very active ^{222}Rn sample measurement" [74].

3.3 The Reference Detector

For the purpose of establishing a control measurement for the detector of choice, it is quite important to analyze its efficiency against a control detector and establish if $\alpha-$particle spectrometry in the RAD-7 detector is the most appropriate for radon progeny measurements. The Liquid Scintillation Counter (LSC) housed at Necsa's Radio-Analysis Laboratories was used for the current study as reference detector. The set-up in Figure 3.4 schematically presents the main components and their functions within an LS counter. Figure 3.4(a) is a flow chart illustrating a water sample mixed with a cocktail, consisting of a scintillator and a solvent. The radiation emitted in the decay of radon and its progeny causes excitation of the scintillator molecules, which subsequently de-excite by emitting light. The emitted light is collected by photomultiplier tubes (PMTs) and converted into electrical pulses that are amplified by auxiliary electronics. The intensity of the scintillation light is linearly proportional to the deposited alpha energy [27, 75].

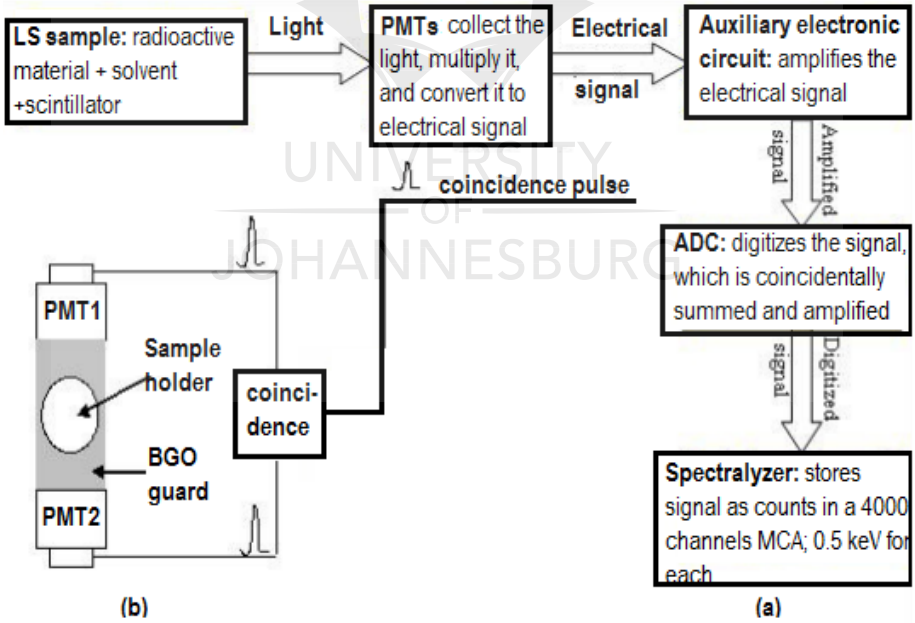

Figure 3.4: Illustration of LSC principle. (a) Flow chart summarizing the main components of a Liquid Scintillation Counter, their respective functions and outputs. (b) Schematic diagram of a detection section of a Packard TRI-LSC system [75].

The signal is processed (digitized and histogrammed) and displayed as a spectrum on a 4 096 channel multi channel analyzer (MCA). The calibration is set so that each channel corresponds to an energy of 0.5 keV. In LS cocktails, the kinetic energy of an $\alpha-$particle is scaled by a factor of about 10 due to the fact that $\alpha-$particles produce pulses of longer duration in the LS cocktail compared to $\beta-$ pulses, e.g. alpha energy of 6.0 MeV appears at 600 keV. The consequence is that in the LSC, the $\alpha-$spectrum overlaps with the high-energy $\beta-$spectrum. Hence, LSCs usually incorporate a pulse-shape discrimination mechanism to distinguish between pulses from alphas and of high-energy betas [75].

3.4 Comparison between RAD-7 and other Detectors

Table 3.1 is the presentation of different detectors that are used to measure the radon concentration in the water [79]. The RAD-H_2O and the Big Bottle are the methods that are used in the RAD-7 instrument. The numbers are typical, and may differ from one laboratory to the other. The precision figures include counting statistics only, with no adjustment for sampling variation or decay of the sample [67]. The most demanding and patient RAD-H_2O operator should be able to reduce the background to less than 0.02 cpm, which will allow for detection limit (DL) and lower limit of detection (LLD) lower than those listed [67].

Table 3.1: Comparison of RAD-H_2O with other methods.

Method	**RAD-H_2O**	**RAD-H_2O**	**Big Bottle**	**[1]LS**	**[2]LC**
Sample Size (ml)	40	250	2500	10	10
Sensitivity (cpm/pCi/l)	0.008	0.05	0.3	0.09	0.05
Background (cpm)	0.02	0.02	0.1	15	0.25
[a]20-min count	40	6		28	9
[a]60-min count	19	3	0.4	16	4
[a]300-min count	7	1	0.18	7	2
[b]20-min count	60	10		41	13
[b]60-min count	29	5	0.6	23	6
[b]300-min count	11	2	0.25	10	3

In Table 3.1; Big Bottle is an accessory for the RAD-7 that enables the user to

measure radon in a 2.5 l water sample with high sensitivity. [1]LS and [2]LC are Liquid Scintillation and Lucas Cell, respectively. a and b are DL, $C = 2(1 + \sqrt{1+2B})$ and LLD, $C = 4(1+\sqrt{B})$, respectively [67].

3.5 Quality Control (QC)

According to N. Vajda, P. Martin and C-K. Kim (Chapter 6 of the Handbook of Radioactivity Analysis (2012), pages 363 – 422), "the general requirements for the competence of testing and calibration laboratories are summarized in the ISO/IEC 17025 (2005) standards [62]. The current section discusses specific QC of $\alpha-$spectrometers and validation of $\alpha-$spectrometric methods" [69].

3.5.1 Quality Control for $\alpha-$spectrometers

The performance of the RAD-7 instrument was verified by counting the sample from the same source in the LSC [69]. The same standard sample containing at least two $\alpha-$emitting radionuclides, which are ^{218}Po and ^{214}Po, was used to to check their energies, the Full Width Half Maximum (FWHM) and the efficiency calibration of the detector or $\alpha-$spectrometer [69]. N. Vajda, P. Martin and C-K. Kim (Chapter 6 of the Handbook of Radioactivity Analysis (2012), pages 363 – 422), "the sample was measured in both techniques under similar conditions which are discussed below. The parameters characterizing the stability of the system are the peak location, the FWHM, and the counting efficiency of a selected radionuclide present in the standard source" [69].

An example of the efficiency data is presented in Figure 3.5 as presented in N. Vajda, P. Martin and C-K. Kim (Handbook of Radioactivity Analysis, pages 363 – 422, 2012), "the measured values are plotted in a control chart as a function of counting date/time. Average values and established control limits are also plotted in each control chart. The 2σ and 3σ deviations from the mean values are regarded as warning and control levels [69]. When measured values are out of the warning-level range, the instrument has to be checked and repaired [69]. If measured values are out of the control limit range, measurements are suspended until

the spectrometer has been repaired. As an example, the efficiency control chart of an alpha spectrometer in shown in Figure 3.5 together with the average values of the measurements and the warning and control levels that were established by the first seven data points" [69].

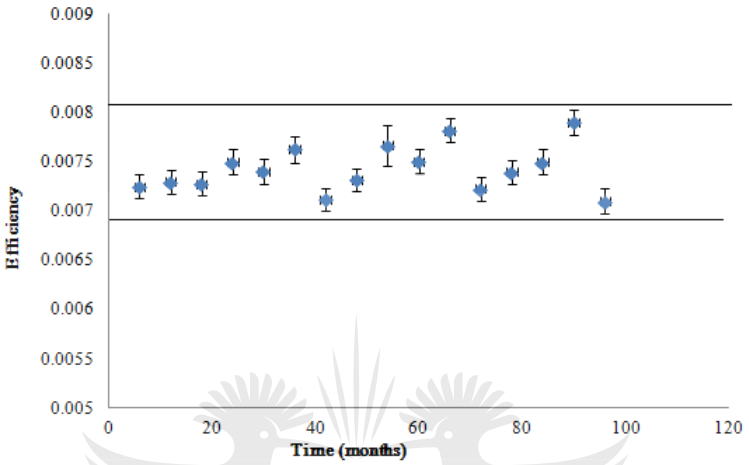

Figure 3.5: Control chart of an alpha spectrometer showing the efficiency data and their uncertainty (1σ) as well as the average values, warning levels ($\pm 2\sigma$ deviation from the average), and control levels ($\pm 3\sigma$ deviation from the average).

3.5.2 *Validation of the Experimental Procedure*

N. Vajda, P. Martin and C-K. Kim (Handbook of Radioactivity Analysis, pages 363 – 422, 2012) describe the validation of the procedure as, "the methods that have been developed at the laboratory, which are nonstandard methods or amplifications and modifications of standard methods, have to be validated to demonstrate that they fit the purposes of application. According to the ISO/IEC 17025 (2005) standards" [69], "the techniques used for the determination of the performance of a method are one of, or a combination of, the following [69]:

1. calibration using reference standards or reference materials;

2. comparison of results achieved with other methods;

3. inter-laboratory comparisons (inter-comparisons exercises or proficiency tests); systematic assessment of the factors influencing the result; and

4. assessment of the uncertainty of the result based on scientific understanding of the theoretical principles of the method and practical experience.

Whenever standards and reference materials with known concentrations of the analytes are available, it is recommended that measurements be carried out using these materials [69]. Results obtained by alpha spectrometry can often be compared with those obtained by other techniques such as mass spectrometry, gamma spectrometry, and liquid scintillation counting [69]. Recently, an increasing number of inter-laboratory comparisons have been organized by national and international institutes, and network laboratories [69]. Although systematic assessment of the factors influencing the result (point 4 above) and evaluation of the uncertainty components (point 5) are extremely important, method validation should not be based exclusively on one of these validation techniques. It is desirable to apply – whenever possible – a combination of the validation techniques (points 1 – 3)" [69].

3.6 Sampling Techniques

A PhD thesis of S.A. Quinn, in 2012 outlined about the technique of sampling, (pages 128 – 154) that, "As radon is a gas, the non-aeration of samples is of critical importance, as water exposed to air during sampling will naturally lose radon to the air phase [93]. Such aeration may therefore result in an underestimation of the total radon content of the source, with no systematic method to correct for such error [93]. For similar reasons, any significant increase in sample temperature during its collection is also undesirable, given the inverse relationship with radon gas solubility [93]. Hence, although the sampling methods may differ according to location, the general protocol for collection and storage of the water sample remained the same in each case" [93].

3.6.1 Standard Sample Preparation

Preparation and measurement of radon aqueous standard solutions are applicable to the continuous radon monitor (CRM) and LSC methods. The standard solution was prepared for both methods and it was used for the analysis to verify the results of the analysis from $\alpha-$spectrometry CRM using LSC. For quality assurance (QA) regarding this approach, the aqueous standard solu tions of different ^{226}Ra activity concentrations were prepared using a reference ^{226}Ra standard solution ACS/DC48/01 of 2003. The initial ^{226}Ra standard activity was used to prepare the master solutions of 2.07 ± 0.07 kBq.g^{-1}.

Figure 3.6 shows the standard samples prepared in the laboratory. Two sets of five known different Radium activity concentrations which were placed in closed vials and kept for 30 days to allow the decay equilibrium between ^{226}Ra ($T_{1/2} = 1600a$), its immediate daughter ^{222}Rn and the four short-lived radon progeny. The presence of ^{210}Pb and its progeny was neglected due to the long half-life of ^{210}Pb ($T_{1/2} = 22.3a$).

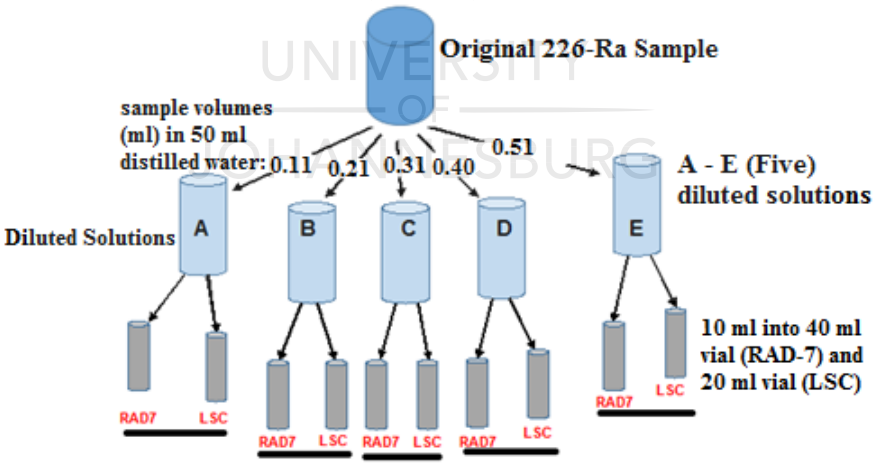

Figure 3.6: Laboratory prepared ^{226}Ra standard samples.

3.6.2 RAD-7 Calibration

The main purpose of this exercise was to evaluate the quality of the radon measurements performed with the portable radon detector RAD-7 [13]. Internal parameters of the measuring chamber of the detector, relative humidity and internal temperature, were thoroughly studied to see how they affected the performance of the detector.

3.6.2.1 Sample Concentration

The detector was calibrated with ^{222}Rn standards prepared (see Figure 3.6) with different concentrations 92.06, 178.46, 262.59 and 336.97 mBq.l^{-1}. The correctness of the results would be established by comparing the measured radon concentration in the samples against the standard sample concentrations. The results were compared with LSC radon detector measurements.

3.6.2.2 Sample Size

The discrete sample volumes of 1, 2, 3, 4 and 5 ml were extracted from the standard solution and were overlaid with distilled water to fill up the vial to determine the effects of sample volumes on the radon concentration. The relationship between the dilution factor and the radon content in the samples was also studied. Verification of the sample volume effects was also done by using the LSC detector.

3.6.2.3 Sample Temperature

Five series of individual experimental runs, each performed at a temperature to determine the effects of sample temperature on the release-rate of radon from the sample. Sample vials were submerged in a water bath to control the temperature during the radon degassing for all five different temperatures [94]. Setups were carried out with the samples temperatures at 4, 9, 14, 19 and 24 °C. To achieve 4 °C, the sample vial was submerged in ice water in the bath whilst the 24 °C temperature was reached by warming the water in the bath.

3.6.3 Sample Height: The Model

In this section, a formula was adopted from I. Csige *et al.* / Radiation Measurements 59, (2013) 201 – 204 and "derived to calculate the radon concentration (C) in the water-filled volume of the sample-holder, measured by the RAD-7 detector as shown in the experimental set-up in Figure 3.7" [87]. The radon concentration in the water will depend on the elevation of the water height in the bottle and diffusion as described by the steady-state transport equation

$$\frac{d^2C(z)}{dz^2} - \frac{\lambda\beta C(z)}{D} + \frac{G}{D} = 0, \tag{3.1}$$

I. Csige *et al.* / Radiation Measurements 59, (2013) 201 – 204, "where D is the radon diffusion coefficient in the water, λ is the radon decay constant and $\beta = (1-m+Lm)\varepsilon$ is the partition corrected porosity taking into account porosity (ε), water saturation (m) and the partition coefficient of radon between the water and air phase, L [87]. On the bottom of the sample-holder, $dC(z)/dz|_{z=0} = 0$. The boundary condition on the top surface of the water sample states that the activity concentration of radon in the water equals that of the air-filled volume of the sample-holder, $C(z=h) = C$" [87].

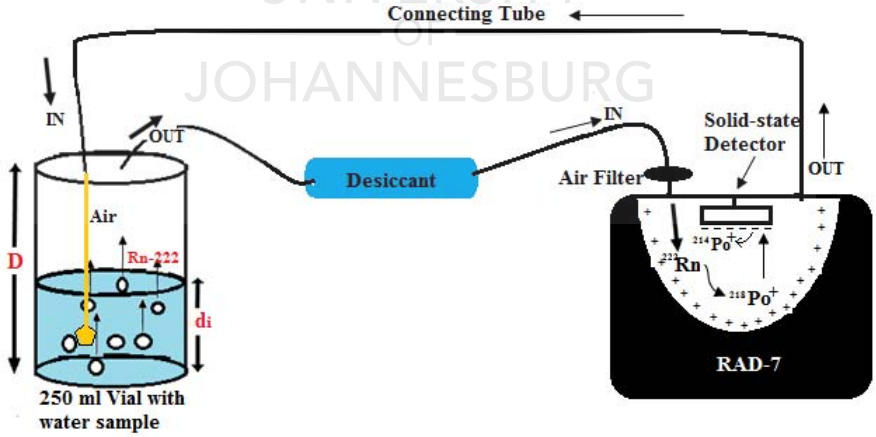

Figure 3.7: Schematic diagram representing the experimental set-up of measuring radon concentration as a function of sample height using an $\alpha-$spectrometer.

I. Csige *et al.* / Radiation Measurements 59, (2013) 201 – 204, "the rate of change of the radon activity concentration in the air-filled volume of the sample-holder is described by the following differential equations, which however, under steady-state conditions, reduce to an algebraic equation" [87]:

$$\frac{dC(t)}{dt} = J\frac{1}{H-h} - \lambda C - \frac{q}{V}C + \frac{q}{2V}C = 0, \tag{3.2}$$

where
J: is the diffusion flux of radon on the top surface of the sample
h: thickness of the sample (m)
q: air flow rate induced by the detector (m^{-3} s^{-1})
V: rest of the volume of the sample holder above the sample (m^3)
λ: decay constant of radon (s^{-1})
H: height of sample holder.

The resultant radon exhalation rate at the water-air interface can then be determined by

$$J = -D\varepsilon\left(\frac{dC}{dz}\right), \tag{3.3}$$

where $dC(z)/dz$ is determined as the solution from Equation 3.1. Using the appropriate boundary conditions, Equation 3.3 becomes

$$J = E \times e^{\rho Ra\lambda L} \times \tanh\left(\frac{H}{L}\right), \tag{3.4}$$

where
E: emanation coefficient ($kg.m^{-1}$)
Ra: radium concentration
ρ: bulk density of material
L: diffusion length, $L = \sqrt{\frac{D}{L}}$.

This system of equations can easily be solved for the radon concentration, C, measured in the air-filled volume of the sample-holder and displayed by RAD-7,

which is expressed as a function of the thickness of the sample [87] (or sample height):

$$C(h) = \frac{G\lambda \times \tanh(k_w h)}{\beta + k_w[2\lambda(H-h)A + q]}, \tag{3.5}$$

where
A: cross-sectional area sample holder (m^2)
C: radon concentration (Bq m^{-3})
G: radon generation rate (Bq m^{-3} s^{-1})
k_w: inverse diffusion length (m^{-1}), $k_w = \sqrt{\lambda\beta/D_w}$
β: partition corrected porosity (–)."

3.6.4 River Samples

River water sampling was done to survey the level of radon in different rivers in the Gauteng Province (see Figure 3.9) during the period from March to November 2014 (Figure 3.8). Water samples were collected from a number of rivers and tributaries for analysis at the Radiation Protection Training Centre (RPTC), Necsa. Before the collection of water samplings, the glass vials were rinsed. Water samples were collected in glass vials that were weighted and lowered beneath the water surface.

(a) Sampling site: Pretoria West.

(b) Sampling site: Irene, Pretoria.

Figure 3.8: Some of the sampling sites in Gauteng.

3.6.5 Decay Correction

As the samples were collected from the rivers, the time between sampling and analysis in the laboratory was required to be compensated for as some radon loss occurs due to decay [82]. The amount of radon loss would be calculated using the decay formula

$$C_t = C_0 e^{-\lambda t}, \tag{3.6}$$

where C_t (Bq.m^{-3}) is the radon concentration at time t (sec), C_0 is the radon concentration at time $t = 0$ and λ is the radon decay constant (s^{-1}) [82]. Given C_t one may obtain the C_0 values that with the addition of exhalation corrections would provide the initial radon concentrations [85].

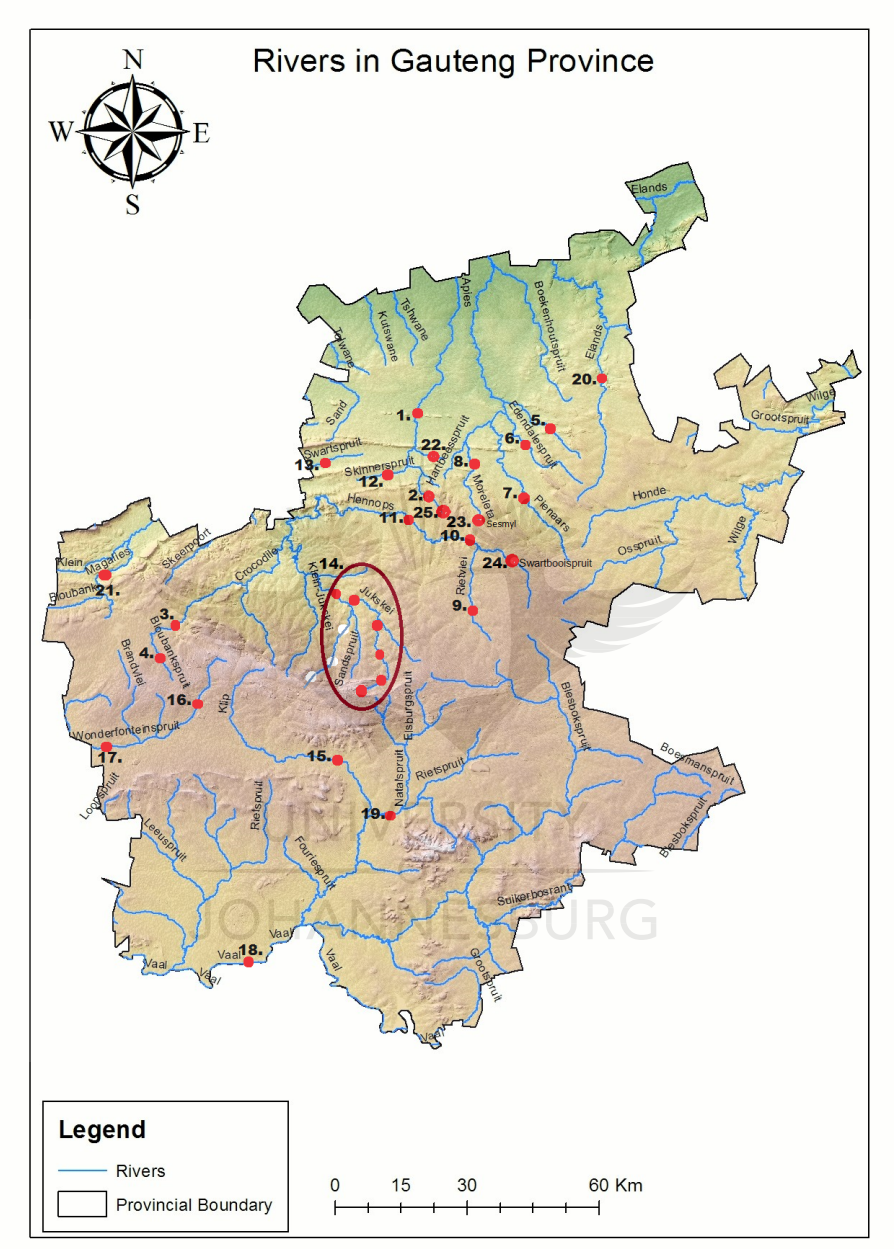

Figure 3.9: The map of the rivers in Gauteng with red dots indicating the approximate locations of selected sites for water samples.

4 Results

4.1 RAD-7 Calibration

4.1.1 Inter-comparison between RAD-7 Instrument and LSC

The validation of the functionality of the detector of choice in the current study, simultaneous measurement using standard samples of radon concentration was carried out to get an inter-comparison between RAD-7 and LSC instruments. The measured values of radon concentration from the two instruments are presented in Table 4.1. The four ^{222}Rn standard sample solutions with known concentrations (Rn-C_{Std}) ranged from 92.1 to 337.0 mBql^{-1} were measured by the two techniques.

Table 4.1: Radon standard sample concentrations (Rn-C_{Std}) measured by RAD-7 (Rn-C_{RAD-7}) and LSC (Rn-C_{LSC}).

Vial no.	Rn-C_{Std} (mBq.l^{-1})	Rn-C_{RAD-7} (mBq.l^{-1})	Rn-C_{LSC} (mBq.l^{-1})
A	92.1	91 ± 7	40 ± 28
B	178.5	136 ± 19	83 ± 20
C	262.6	242 ± 27	149 ± 15
D	337.0	315 ± 19	255 ± 11

The measured concentrations varied from 90.7 ± 7 mBq.l^{-1} to 314.7 ± 25 mBq.l^{-1} and 40.3 ± 28 mBq.l^{-1} to 255.5 ± 11 mBq.l^{-1} for the $\alpha-$spectrometry technique and the LSC, respectively. Figure 4.1 shows the results of this inter-comparison experiment performed in the current study. It was observed that the response of $\alpha-$spectrometry technique closely matched with that the standard sample by 0.9

factor while the LSC was at 0.6. Figure 4.2 shows the correlation between the measured values of radon concentration by the $\alpha-$spectrometry technique and the LSC.

The variations in measured radon concentrations from the RAD-7 instrument were within 10 % of the standard sample, while the LSC was constantly low and its measured radon concentrations varied about 56 % from the standard sample. It is clear from the measurements that the $\alpha-$spectrometry in the RAD-7 instrument can be used for laboratory and field determination of radon concentrations. The method of $\alpha-$spectrometry makes the RAD-7 instrument more reliable in comparison with other radon monitors. Therefore, the RAD-7 instrument can be used in low and high radon environment, it is portable and can be useful for a general survey even in the dwellings or fields.

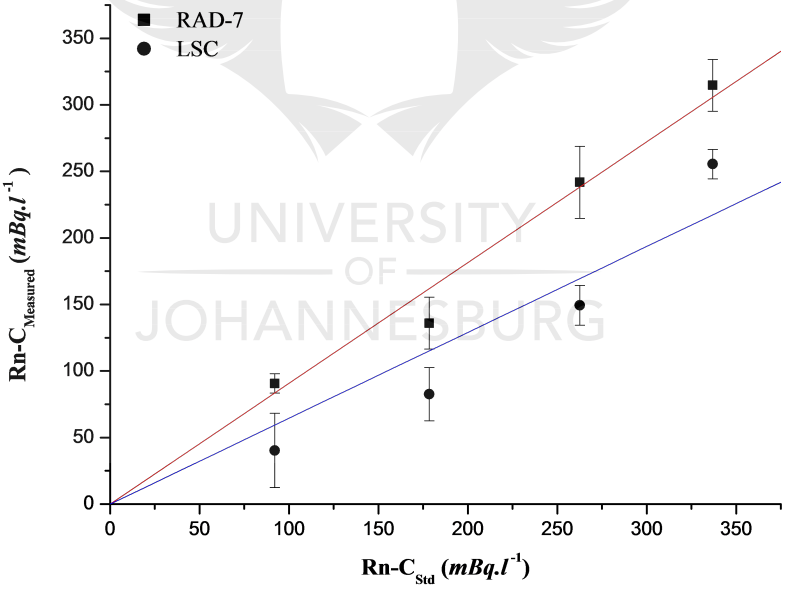

Figure 4.1: Measured radon concentration by $\alpha-$spectroscopy in a solid-state detector of the progeny and luminensce from the integral of all charged particles released.

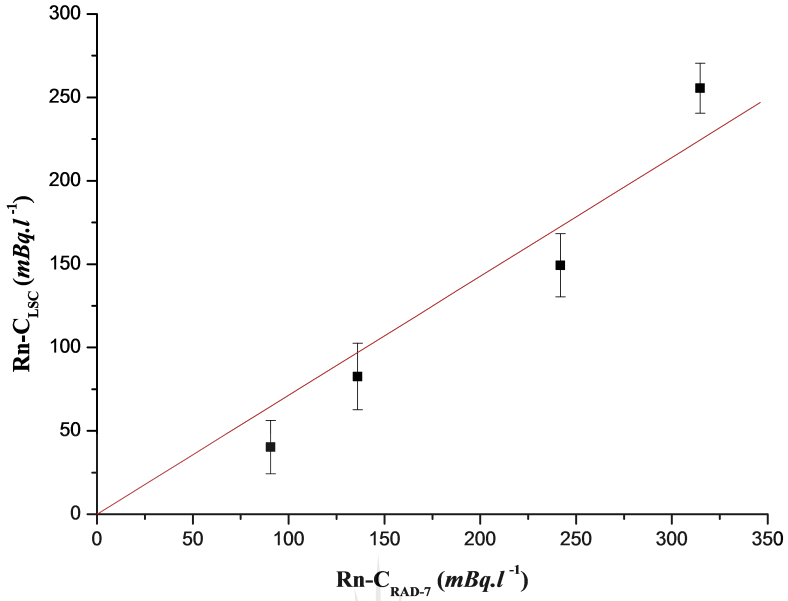

Figure 4.2: Correlation between the RAD-7 instrument and the LSC detectors.

4.1.2 Spectra Analysis

When charged, ^{218}Po and ^{214}Po ions impact onto the surface of the detector in the internal cell of the RAD-7 instrument, this produces a signal which when accumulated and stored, resulted in a spectrum with an energy scale from the calibration (Figure 4.3). The spectrum scale divided into 200 channels (of 0.05 MeV each) and selected regions grouped into 8 energy windows of which the four major ones were A, B, C and D. The two peaks with resolutions (FWHM) 19 keV (^{218}Po) and 21 keV (^{214}Po) shifted to the right by 50 keV and 210 keV, respectively.

Figure 4.4 presents the energy spectrum of ^{222}Rn and its progeny for the same standard sample of 92.06 mBq.l^{-1}, measured with the LSC instrument with three peaks of ^{222}Rn, ^{218}Po and ^{214}Po with the energy shifted to the right by almost 2 MeV. The cause of the shift of the peaks was due to energy loss in the transfer from solvent to solute or the attenuation of light photons in the solution. The scintillometer efficiency factor (1.86) obtained here was over the range 0 – 10 240 keV

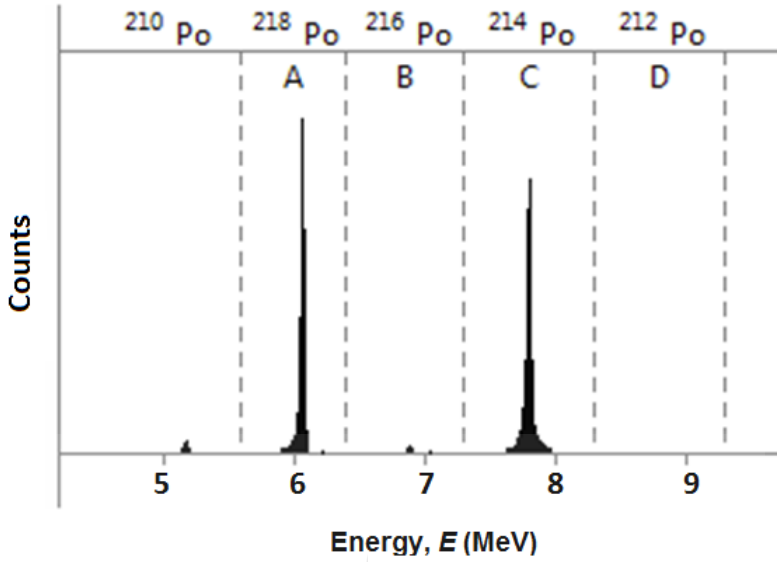

Figure 4.3: Spectroscopy of the standard sample (92.06 mBq.l^{-1}). RAD-7 instrument alpha spectrum showing peaks of ^{218}Po and ^{214}Po.

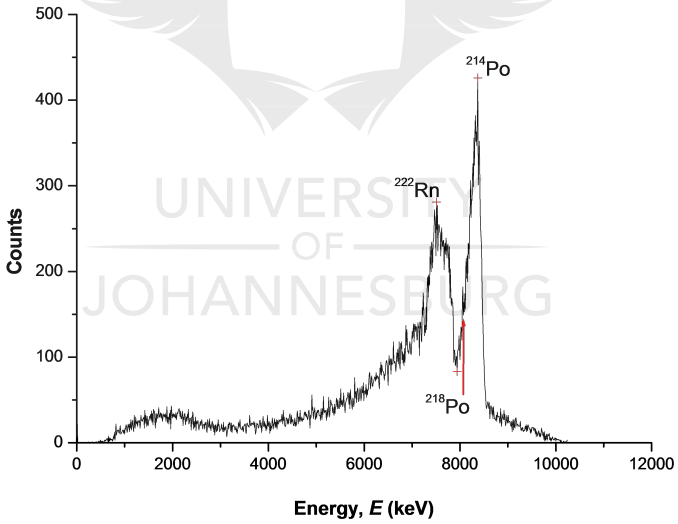

Figure 4.4: Energy spectrum obtained for determining ^{222}Rn, ^{218}Po and ^{214}Po activity and concentration.

energy window [69], chosen for the refined $\alpha/\beta-$ separation capability and lower background. The spectrum was characterized by a relatively poor resolution with a FWHM of 166 keV and the variation of the resolution as a function of energy is

more than in semiconductor $\alpha-$spectrometry [69].

This resolution does not allow the detection of the individual alpha lines belonging to the various $\alpha-$emitting isotopes. In Figure 4.4 the alpha radiation of ^{218}Po and ^{214}Po appears in a single common peak and cannot be resolved [69]. The energy-tailing was caused by Compton Scattering. The summary of QCs between RAD-7 and LSC in this study are presented in Table 4.2.

This discussion further empahises the preference of selecting the RAD-7 instrument for radon concentration determination over the LSC instrument, and it lends additional credibility to the results that will be obtained, as the survey instrument is more reliable. Therefore, the method of $\alpha-$spectrometry technique as embodied in the RAD-7 instrument was an appropriate choice as it is more precise and less susceptible to interferences than other instruments, for the task in hand.

Table 4.2: The parameters characterizing the stability of the system.

Parameters / Detectors	**RAD-7 Detector**	**LSC Detector**
Peak position (MeV)	6.05 (^{218}Po)	7.51 (^{218}Po)
	7.90 (^{214}Po)	8.31 (^{214}Po)
Resolution (FWHM) (keV)	18.61 (^{218}Po)	166
	20.93 (^{214}Po)	
Counting efficiency (%)	90.03	50.6

4.2 Effects of Varying Sample Geometry Parameters on the Radon Concentration

Figure 4.5 is the representation of the sample volume, V_s (ml) and the sample height, h (mm) in the sample bottle (vial). Sections 4.2.1 and 4.2.2 show the measured values of radon concentration as a function of V_s and h, respectively. The volume of air, V_a is the air-filled part of the vial with volume: $V_a = A(L-h)$, where A is the surface area of the cylindrical vial and L is the height of the vial. The standard sample with the radon concentration of 426.2 mBq.l^{-1} was used.

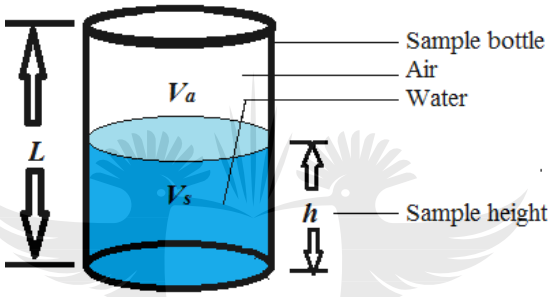

Figure 4.5: The figure representing the sample bottle (vial) used in this study. Where V_s, V_a and h are water sample volume, air volume (above the sample level) and sample height, respectively.

4.2.1 Effects of Sample Volume

Table 4.3 shows the experimental results of the effect of five different volumes of the water sample that was collected from the Hartbeespruit River, V_s (1, 2, 3, 4 to 5 ml) on the radon concentration in the sample. The results show that when the sample volume increased, the radon concentration slightly increased. Figure 4.6 the radon concentration as a function of the sample volume. The radon concentration increased by a factor of 4 between the first sample volume which was 1 ml to the last volume of 5 ml. Ideally, the concentration was suppose to remain the same because all five volumes were taken from the same sample. Since the basic volume of the air chamber in the RAD-7 instrument, desiccant and tubes are fixed, any variation of air volume is dependent on V_s in the vial [1].

Table 4.3: The effects of varying the standard sample volumes measured on radon concentration.

Vial no.	V_s (ml)	Rn-C_{River} (mBq.l^{-1})
A	1	16 ± 5
B	2	17 ± 5
C	3	19 ± 4
D	4	19 ± 6
E	5	23 ± 4

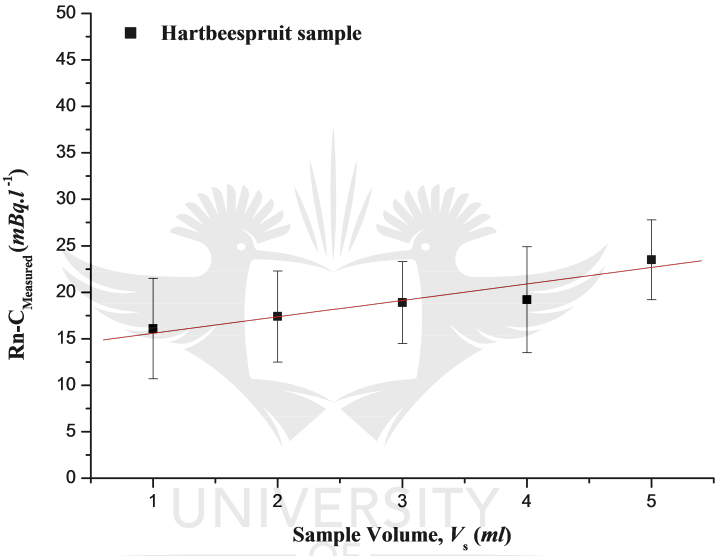

Figure 4.6: Plot of radon concentration of standard and river sample against the sample volume.

The experimental results indicated that the volume of water sample, V_s had a little effect in the determination of radon concentration in water. Nevertheless, the size of the volume used should be kept constant in the measurements to avoid this systematic effect.

4.2.2 Effects of Sample Height

Table 4.4 shows the effects of sample height, h, on the radon concentration using the RAD-7 detector. The height of the sample was increased in intervals of 10 mm resulting in a non-linear increase of radon concentration. Radon concentration of the samples collected from the Hartbeespruit River ranged from 0.72 ± 0.22 mBq.l^{-1} to 2.13 ± 0.38 mBq.l^{-1} while varying the sample height in the sample-holder.

Table 4.4: The effects of varying the sample height, h on radon concentration the in the sample-holder.

Vial no.	h (mm)	Hartbeesspruit$_{RAD-7}$ (mBq.l^{-1})
A	10	72 ± 22
B	20	137 ± 38
C	30	174 ± 44
D	40	194 ± 45
E	50	209 ± 43
F	60	213 ± 38

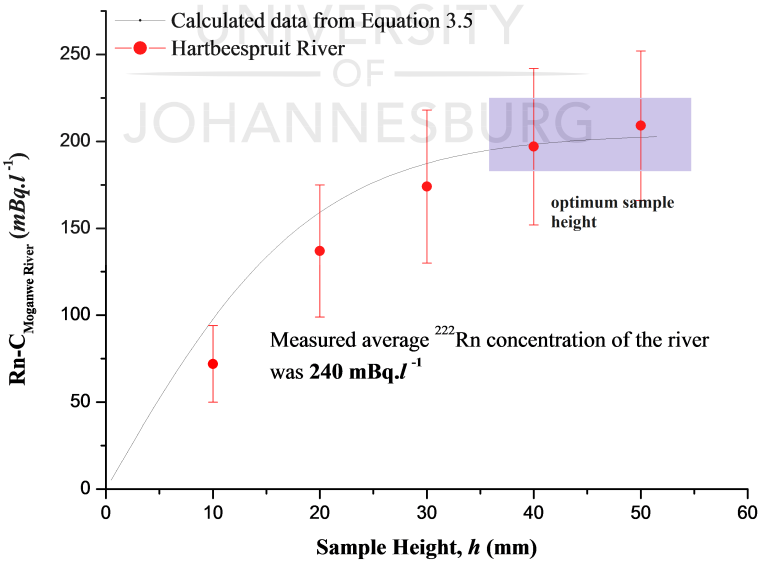

Figure 4.7: Radon concentration as a function of sample height, h in the sample-holder.

The radon concentration measurement at different values of h, is graphically presented in Figure 4.7 together with the curve of the best fit of the model in Section 3.6.3 as summarised by formula 3.5. The mathematical model of the measurement technique described the apparent change of the concentration of the activity as a function of sample height, h well. The validation of this model of the experiment was established that the response of the RAD-7 instrument measuring the radon concentration as a function of the sample height. For the purpose of measuring large number of samples, the study has determined an optimal sample height of 40 mm. The results were consistent with the optimal sample height of 50 mm from the experiment conducted by I. Csige *et al.* / Radiation Measurements 59 (2013) 201 – 204 [87].

4.3 Effects of Internal Temperature and Relative Humidity

A radon concentration was detected in the water samples from the Walkerspruit River with an average radon concentration of 35 mBq.l^{-1} using RAD-7 instrument at different relative humidity (RH) and internal temperature (T_{int}) values, as shown in Table 4.5. The effects of increased RH and T_{int} from 14 % to 24 % and 21 °C to 22 °C respectively have an impact of the functionality of the detector in terms of its counting efficiency. It was observed that the radon concentration varied from 34.2 $\pm$ 8 mBq.l^{-1} to 26.6 $\pm$ 1.5 mBq.l^{-1} while the relative humidity and temperature inside the RAD-7 instrument varied. The average radon concentration measured in this sample was 31.2 $\pm$ 7 mBq.l^{-1}.

Table 4.5: The effect of relative humidity and internal temperature on the response of the RAD-7 instrument during the measurement period.

Measurement time (min)	T_{int} (°C)	RH (%)	Rn-C (mBq.l^{-1})
5.0	20.6 $\pm$ 0.8	13.0 $\pm$ 1.8	34.0 $\pm$ 8.0
13.0	21.0 $\pm$ 0.2	18.0 $\pm$ 1.1	34.0 $\pm$ 9.0
21.0	21.5 $\pm$ 0.2	21.0 $\pm$ 0.5	31.0 $\pm$ 7.0
32.0	22.0 $\pm$ 0.3	22.0 $\pm$ 0.5	30.0 $\pm$ 7.0
36.0	22.4 $\pm$ 0.2	24.0 $\pm$ 0.5	27.0 $\pm$ 2.0

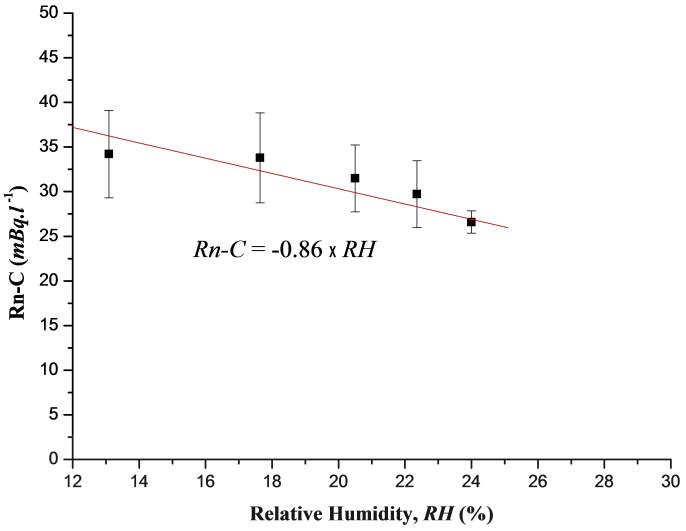

(a) The effect of varied relative humidity on the radon concentration measured by the $\alpha-$spetrometry method of the Walkerspruit water sample.

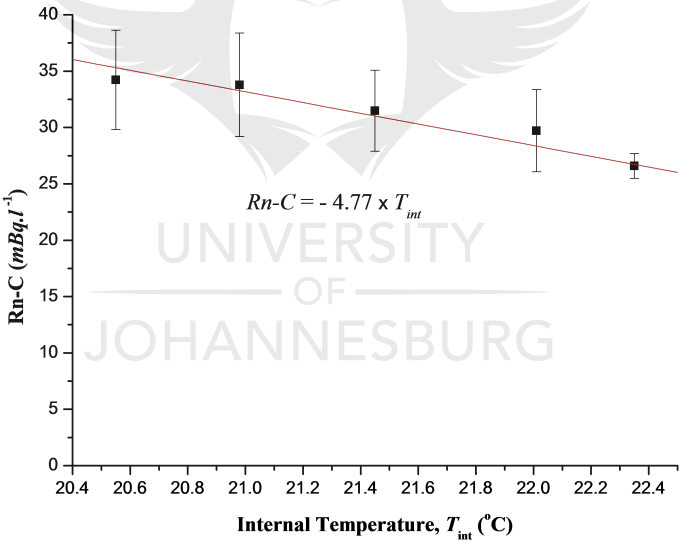

(b) The effects of internal temperature on the radon concentration measured by the RAD-7 instrument.

Figure 4.8: Plots representing the effect of the internal cell parameters on the radon concentration of the Walkerspruit water sample.

The internal temperature (T_{int}) and bias voltage affect the measurement of radon concentration when using the RAD-7 instrument. The performance and characteristics of the electrostatic collection rate of ^{222}Rn by the detectors are dependent on the charge of the uranium progeny atoms. In the RAD-7 detector, a high electric field of 2 keV in the detection chamber propels the positively charged ^{218}Po and ^{214}Po, onto the detector (Figure 3.2) [98]. The movement can be hindered by an increase in relative humidity, *RH*, inside the detection chamber. According to Batta (Radon in the DRIFT-II, 2015), "Being a polar molecule, water vapour attracts ions and hence reduces the instrument's sensitivity by preventing radon daughters from reaching the sensitive part of the detector [84]. As the *RH* rises, radon concentration decreases, Figure 4.8a. A similar reasoning based on the survival of ions in their charged state would apply for the internal temperature variable." [84]

The effect of the relative humidity at the measurement was caused mainly from the continuous circulation of incoming air to the detection chamber of the RAD-7 instrument [84]. Figures 4.8a and 4.8b showed that when *RH* and T_{int} increase in the internal cell of the detector, less radon concentrations were counted by the detector [84]. The inverse relationship between ΔRH and ΔT_{int}, and the radon concentration measured by the detector is presented in both figures.

The results in Table 4.5 proved that *RH* has an influence over radon detection. Figure 4.8a further shows that the highest radon concentration occurs at the lowest *RH* percentage. A correction for the effect of *RH* at the time of the measurement was applied to tests in which $RH \geq 13$ % was done by using Equation 4.1 below, [84],

$$C_f = C_i \times \frac{100}{116.67 - 1.1 \times RH}, \tag{4.1}$$

where C_i and C_f represent Rn activity before and after the *RH* correction, respectively. The corrected concentration, C_f is represented by Figure4.9.

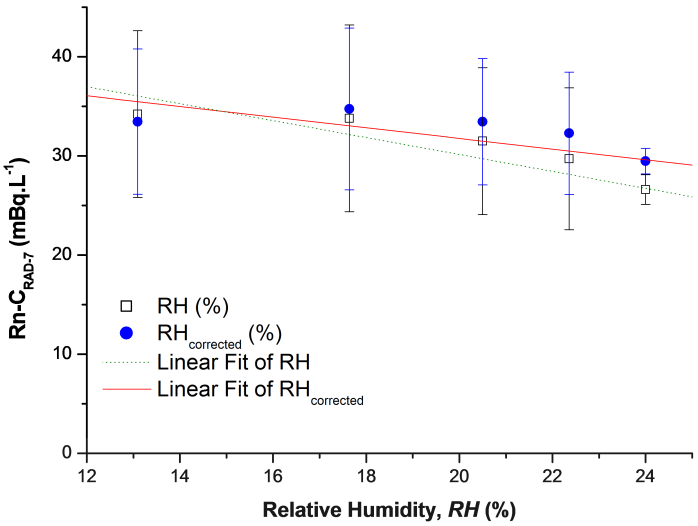

Figure 4.9: The effects of meteorological parameters in the internal cell of the RAD-7.

4.4 *Effects of measuring Time on Radon Concentration in the Measuring Chamber*

Since the RAD-7 instrument is a counting system in a closed air-loop, only decay and leakage would lead to lower concentrations over time [95]. The plotted data in Figure 4.10 shows that there was a reduction of the radon activity concentration during the counting periods which were about 85 hours (3.5 days). The theoretical loss was calculated by the use of the radioactive decay equation, where A_0 is the initial radon concentration; A_t the observed concentration at time, t and λ is radon decay constant (0.2 d^{-1}) [95].

$$A = A_0 e^{-\lambda t}, \tag{4.2}$$

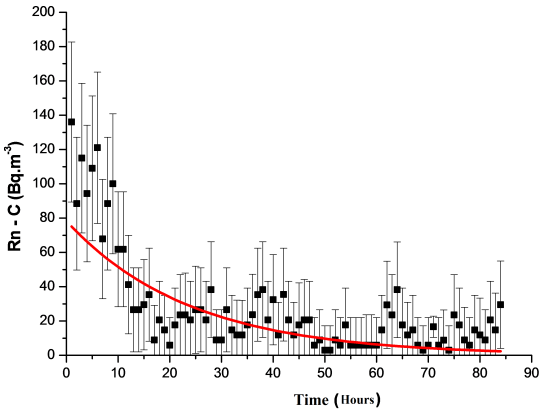

Figure 4.10: Rise time of activity of ^{222}Rn and its decay products in the RAD-7 instrument. 85 hours of counting time.

4.5 Radon Concentrations in Water from the Various Rivers in Gauteng

The measurements using the RAD-7 instrument, of some river water samples for the general survey of the radon concentration level in water with the meteorological parameters of temperature (T_{int}) and relative humidity (RH) at the sample volumes of 250 ml for some of the rivers in Gauteng are listed in Table 4.6 and Figure 4.11. A color temperature scale has been used to indicate the radon concentration. The measured sites in the rivers are therefore represented by colored dots, where the key of the left indicates the radiation concentration color assigned for each bin in a concentration sub range. All samples were measured using the $\alpha-$spectrometry technique in the RAD-7 instrument but two were found to be below the minimum detectable limit (MDL) of the instrument which is 0.4 Bq.l^{-1}.

An insert indicates the mining activity nearby and its expected radiological implications. Therefore in Figure 4.11 from the GDARD (Gauteng Mine Residue Areas Strategy, 2012), "radioactive (red), non-radioactive (green) and undetermined (blue-very few) Mining Residue Areas (MRAs) in Gauteng, on sun-shaded Shuttle radar topography mission (SRTM) topography with the main drainages (blue streams), dams/lakes (blue) and catchment divides (brown) are also shown [81]. The concentration of radioactive MRAs in the Witwatersrand headwater areas of

Table 4.6: Results of ^{222}Rn concentrations and the average annual effective dose due to the ingestion (ED_{ing}) of radon in river water samples (Masevhe *et al.*, J Environ Anal Toxicol 2017, 7:4).

ID no	Sampling site	RH (%)	T_{int} (°C)	^{222}Rn (Bq.l^{-1})	ED_{ing} (μSv.a^{-1})
1	Apies1	16.0	20.3	1.2 ± 0.2	8.6
2	Apies (PTA Central)	18.3	21.6	0.9 ± 0.3	6.4
3	Bloubankspruit 1	14.7	30.4	0.6 ± 0.2	4.4
4	Bloubankspruit 2	13.4	28.2	0.4 ± 0.1	3.1
5	Edendalspruit 1	20.0	20.3	2.6 ± 0.2	19
6	Edendalspruit 2	20.0	20.3	1.9 ± 0.4	14
7	Pienaarsriver	19.4	22.2	2.8 ± 0.2	20
8	Moreleta	21.0	20.2	4.9 ± 0.3	36
9	Rietvlei	29.7	20.7	1.1 ± 0.1	7.8
10	Hennops River 1	23.4	18.8	2.8 ± 0.2	20
11	Hennops River 2	24.0	21.9	3.4 ± 0.6	25
12	Skinnerspruit	23.0	23.6	0.4 ± 0.2	2.6
13	Swartspruit	23.5	22.0	0.5 ± 0.3	3.6
14	Jukskei River	22.0	23.0	1.2 ± 0.2	8.9
15	Klip River	22.9	24.9	0.5 ± 0.1	3.4
16	Muldersdrift Se Loop	17.8	30.9	1.1 ± 0.2	11
17	Wonderfontein	19.9	27.3	0.4 ± 0.1	2.8
18	Vaal River	21.2	26.8	0.1 ± 0.1	0.9
19	Natalspruit	23.5	25.4	2.8 ± 0.2	21
20	Elands	26.4	24.2	0.5 ± 0.1	3.9
21	Magaliesriver	13.5	29.0	0.8 ± 0.2	6.2
22	Hartebeespruit	22.5	26.3	0.3 ± 0.1	8.1
23	Sesmylspruit	22.0	18.5	0.8 ± 0.1	4.9
24	Swartbooispruit	28.8	24.3	0.9 ± 0.1	6.4
25	Walkerspruit	21.5	21.8	1.1 ± 0.7	9.2

the Vaal catchment is evident, with some overlap into the Limpopo (Crocodile West) headwaters near Krugersdorp" [81].

Figure 4.16 is therefore an important figure. At a single glance, it shows the results of this survey which can also be correlated to the local anthropogenic activities, and which are related to the hypothesis of this thesis. The radon concentration hotspots are not correlated to drainage of mining areas, therefore the data is consistent

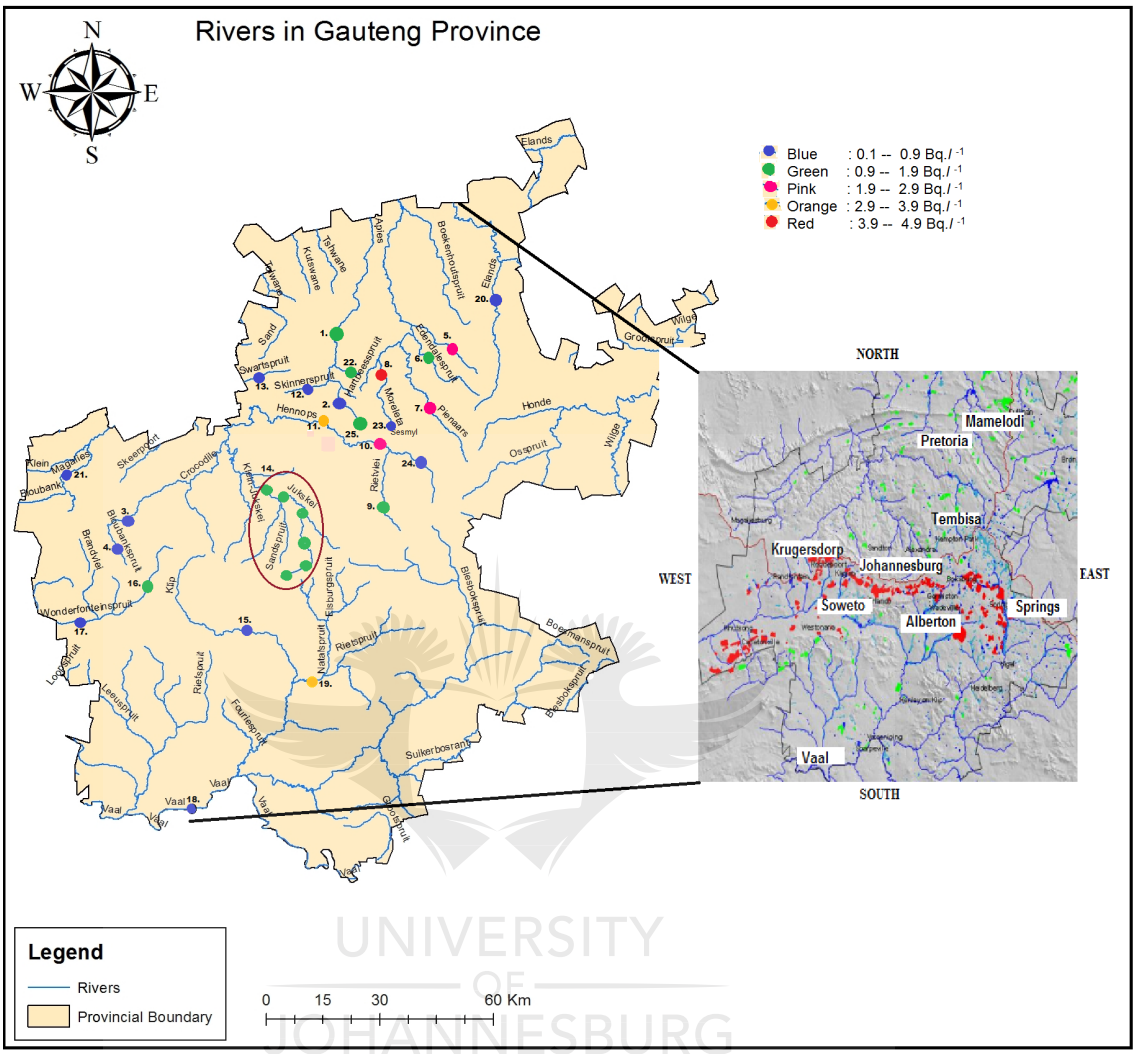

Figure 4.11: A map of Gauteng Province showing the distibution of radon concentration in the water from some of the rivers in Gauteng and the Mining Residue Areas (MRAs), insert.

with an interpretation that local natural geological conditions are more pertinent than anthropological consideration.

The reason for the variation in radon concentrations could be due to geological environment variation and with its mining history in different regions in Gauteng. Radon is decay product of uranium, which is a heavy metal found in all rock

and soil. The general survey of different rivers show that the radon concentration in the rivers around Pretoria areas are slightly higher than those in Johannesburg areas as indicated in Figure 4.12. The highest recorded radon concentration in Pretoria and in Johannesburg were 1 Bq.l^{-1} and 0.5 Bq.l^{-1}, respectively with the average radon concentration of 1.31 Bq.l^{-1} for Pretoria rivers while the average radon concentration in the Johannesburg rivers is 0.36 Bq.l^{-1}.

Figure 4.12 presents the data in Table 4.6 as a bar chart, showing the variation of radon in water samples from different rivers across the province. The level of radioactive of ^{222}Rn for water samples, as shown in Table 4.6, range from 0.1 $\pm$ 0.1 Bq.l^{-1} for sample No. 18 in the Vaal River (Vanderbijlpark) to 4.9 $\pm$ 0.3 Bq.l^{-1} for sample No. 8 in Moreleta (Pretoria East). The average radon concentration of the general observation for the sampled rivers in the Gauteng Province as tabulated in Table 4.6 was 1.4 $\pm$ 0.2 Bq.l^{-1}. The corresponding annual effective dose due to the ingestion of radon (last column) varied from 2.70 μSv.a^{-1} to 20.94 μSv.a^{-1} with an average value of 9.02 μSv.a^{-1}.

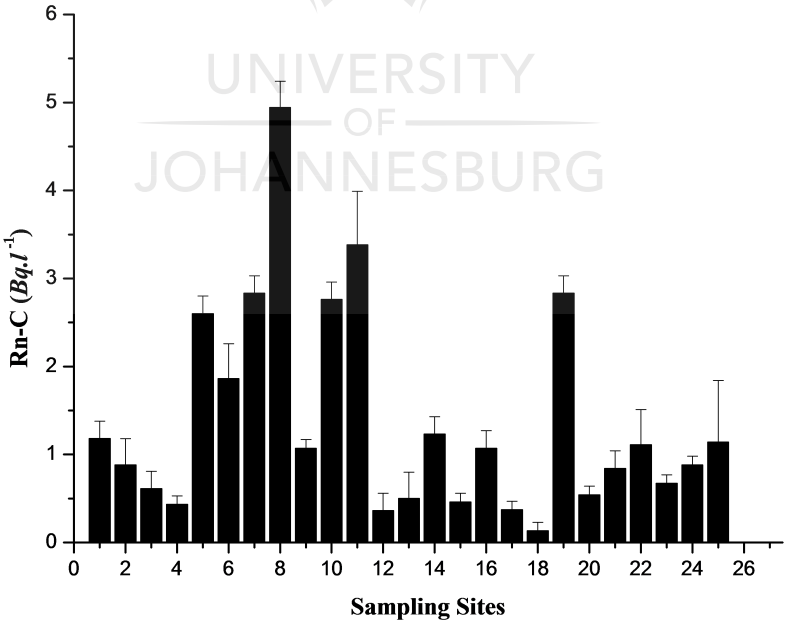

Figure 4.12: General survey of radon concentration in the water from some of the rivers in Gauteng.

Figures 4.13 and 4.14 show the sampling points from Jukskei River and an increment of radon concentration as the river progresses downstream. Table 4.7 shows the radon concentrations in Bruma Lake was 0.4 $\pm$ 0.2 Bq.l^{-1} and it increased to 2.3 $\pm$ 0.4 Bq.l^{-1} in Kyalami Bridge which is 33 km downstream. Similar trends were observed in the Hennops and Walkerspruit Rivers, were the measured radon concentration increased from 2.8 $\pm$ 0.2 Bq.l^{-1} (Hennops River 1 in Centurion Lake) to 3.4 $\pm$ 0.6 Bq.l^{-1} (Hennops 2 in Broederstroom area) and 1.1 $\pm$ 0.7 Bq.l^{-1} (Waterkloof) to 2.5 $\pm$ 0.6 Bq.l^{-1} (Magnolia Park in Pretoria) as show in Table 4.8.

Table 4.7: Accumulation of radon concentration on Jukskei Rivers in Johannesburg .

Sample No.	Description Sampling site	C_{Waterl} (Bq.l^{-1})
1	Bezuidenhout valley	0.4 $\pm$ 0.2
2	Bruma Lake	0.4 $\pm$ 0.2
3	Gillooly's Farm	0.8 $\pm$ 0.3
4	Edenvale	1.6 $\pm$ 0.3
5	Modderfontain	1.5 $\pm$ 0.5
6	Malboro (Alexandra)	1.4 $\pm$ 0.2
7	Buccleuch	1.6 $\pm$ 0.3
8	N1 Bridge (Midrand)	1.9 $\pm$ 0.5
9	Kyalami Bridge	2.3 $\pm$ 0.4

Table 4.8: Accumulation of radon concentration on Hennops and Walkerspruit Rivers in Pretoria .

Sample No.	Description of Sampling site	C_{Waterl} (Bq.l^{-1})
1(a)	Walkerspruit1	1.1 $\pm$ 0.7
1(b)	Walkerspruit2	2.5 $\pm$ 0.6
2(a)	Hannops1	2.8 $\pm$ 0.2
2(b)	Hannops2	3.4 $\pm$ 0.6

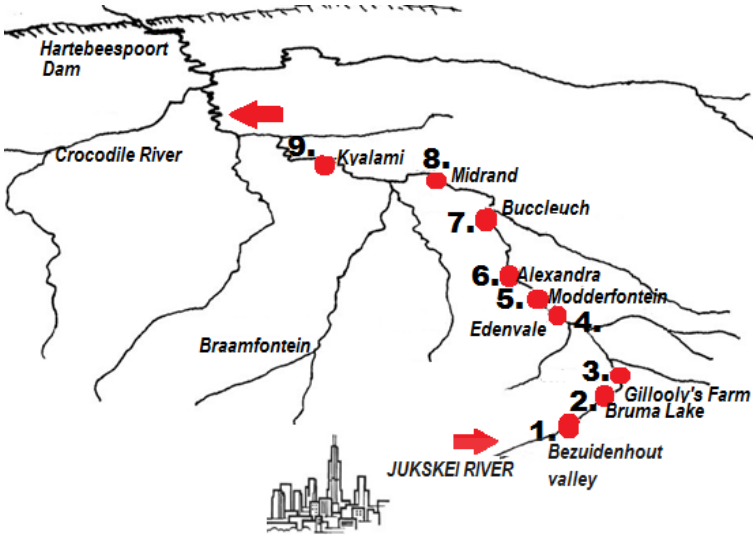

Figure 4.13: Map of Jukskei River, red dots indicate approximate locations of selected sites for water samples and red arrows show the water flow direction.

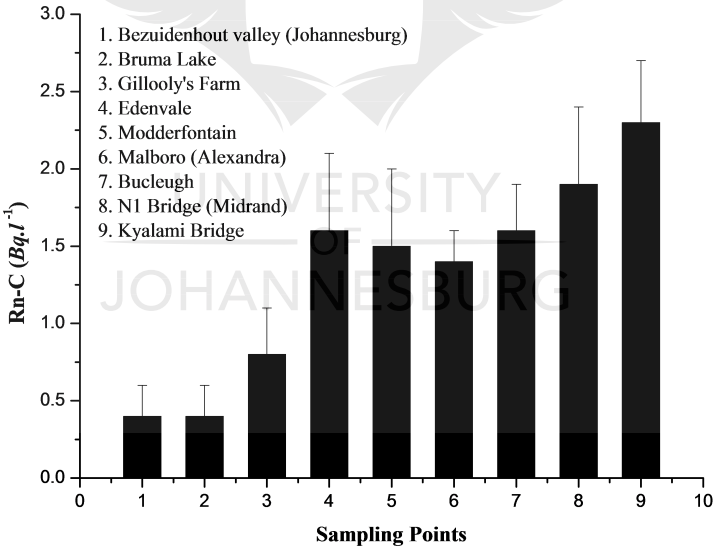

Figure 4.14: The graph shows the radon concentration increment downstream of Jukskei River.

The results of this survey show that radon concentration increase downstream. The reason for this could be due to radon accumulation as a result of radon carried

by water when river flows and the continuous release from the bedrock and soil.

4.6 The Regional Distribution of Radon Concentration in the Gauteng rivers

Figure 4.15 shows the percentage contribution to the total radon concentration in the water samples from the general survey conducted in the current study. The Gauteng North appears to have contributed about 48.1 percent of the total contribution to the average value of radon concentration of 1.11 Bq.l^{-1}. The average radon concentration in the current study was found to be 1.4 $\pm$ 0.2 Bq.l^{-1} and below the results of the water from mining areas (in the Witwatersrand, Johannesburg) with radon concentration in the range from 1.5 to 70 Bq.l^{-1} [53]. The reason for this outcome could be that the current study focused on the river water and not on the groundwater or the water from the rivers around the mining areas.

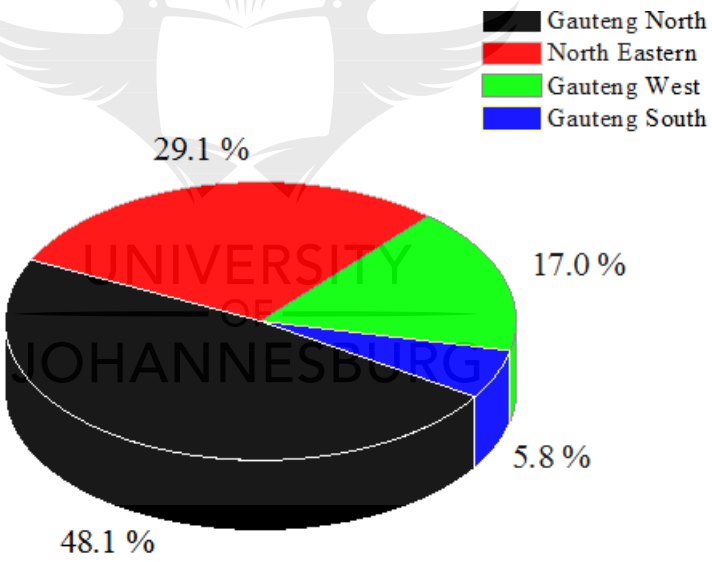

Figure 4.15: Percentage contribution to the total radon concentration of water samples from the rivers in Gauteng in this study.

Table 4.9: General Survey of Radon Concentration and effective dose rate from the rivers in Gauteng West.

Sample ID	Description (River Name)	RH (%)	T (°C)	C_{Waterl} (Bq.l^{-1})	ED_{ing} (μSv.a^{-1})
WNF	Wonderfontein	20	27	0.4 ± 0.1	3
MLD01	Muldersdrift Se Loop	18	31	0.7 ± 0.2	5
MLD02	Muldersdrift	17	29	1.5 ± 0.3	1
BBS01	Bloubankspruit	15	30	0.8 ± 0.2	6
BBS02	Bloubankspruit (Lanseria)	15	31	0.4 ± 0.2	3
MGL	Magaliesriver	14	29.	0.8 ± 0.2	6

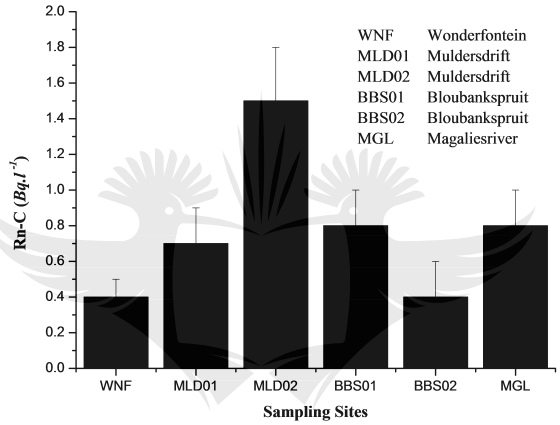

Figure 4.16: General Survey of Radon Concentration and effective dose rate in the water from some of the rivers in West Rand.

4.6.1 Measurement along the Gauteng West Rivers

Results of the measurements performed on the water samples from the western side of Gauteng were respectively presented in Table 4.9 and Figure 4.18 as distribution of the measured radon concentrations, where the average value was 0.8 Bq.l^{-1}. The values of radon concentrations have a wide range, between 0.4 and 1.5 Bq.l^{-1}. This range shows an increase of radon concentration measured at two different points of Muldersdrift area having a distribution with a maximum in point MLD02 which has a value of 1.5 Bq.l^{-1}. Two samples were found to be at the level of MDL of the RAD-7 instrument. The difference in the order of magnitude between samples as presented in Table 4.9 is likely caused by the fact that

the measurements were performed in different rivers which originated from different geological environments. Figure 4.17 shows a clear relationship between the measured radon concentrations and the underlying geological features such as the uranium content and permeability of rock and soil. The important factor causing elevated radon concentration in the Northern part of the City of Johannesburg was the uranium content of sedimentary rocks composed primarily of the mineral dolomite with high permeability and porosity and fractured rocks. The insert shows that the radon concentration measured from Klip River was 0.5 $\pm$ 0.1 Bq.l^{-1} and Jukskei River was 1.2 $\pm$ 0.2 Bq.l^{-1}, were found to be below the concentration from Hennops River of 3.4 $\pm$ 0.6 Bq.l^{-1} situated on dolomatics area.

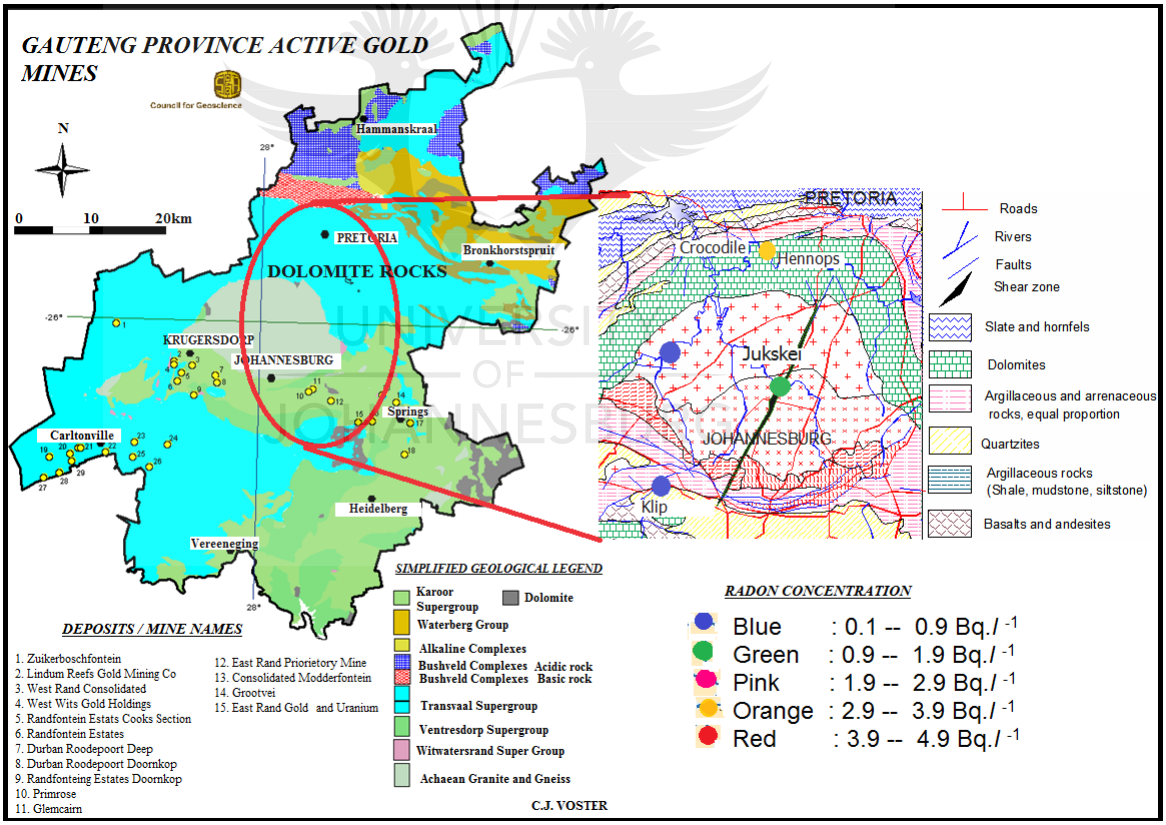

Figure 4.17: Geological map of with active gold mines and deposits in the Gauteng Province, South Africa [90] (Council for Geoscience).

Figures 4.11 and 4.17 shows that the radon concentration hotspots are not correlated to drainage of mining areas, therefore the data is consistent with an interpretation that local natural geological conditions are more pertinent than anthropological consideration. Therefore, the study shows that the local geological environment is important for the release of radon to the rivers and that because radon is rapidly released from water to the atmosphere, it is not entirely unexpected in the rivers.

4.6.2 Measurement along the rivers in Pretoria Central and the South

Results of the measurements performed on the water samples as presented in Table 4.10 and Figure 4.18 as distributions of radon concentrations with the average value of 1.4 Bq.l^{-1}. The average value is about 57 % higher that the average concentration of radon in the western side of the province as shown in Table 4.9. It can be seen that the two sampling points of Hennops River contributed the radon concentrations of 1.9 and 3.6 Bq.l^{-1}. The reason for the higher values of radon concentration might be the result of the build up as one proceeds downstream as was highlighted by the discussion on the results for the Jukskei River in Figure 4.14.

Table 4.10: Radon Concentration and effective dose rate from the rivers in the Midrand and Centurion South.

Sample ID	Description (River Name)	RH (%)	T (°C)	C_{Waterl} (Bq.l^{-1})	ED_{ing} (μSv.a^{-1})
RTS01	Rietspruit 1	30	21	1.1 ± 0.1	7.8
RTS02	Rietspruit 2	30	21	1.1 ± 0.1	7.8
SWB	Swartbooispruit	29	24	0.9 ± 0.1	6.4
SSM	Sesmylspruit	28	19	0.7 ± 0.1	4.9
OLF	Olifantspruit	26	24	0.5 ± 0.1	3.9
JKS01	Jukskei(Diepsloot)	24	21	1.2 ± 0.2	9.0
HNP01	Hannops (R511)	23	26	1.9 ± 0.2	14
HNP02	Hannops (Centurion)	21	24	3.6 ± 0.3	27
APS	Apies	22	25	1.2 ± 0.2	13

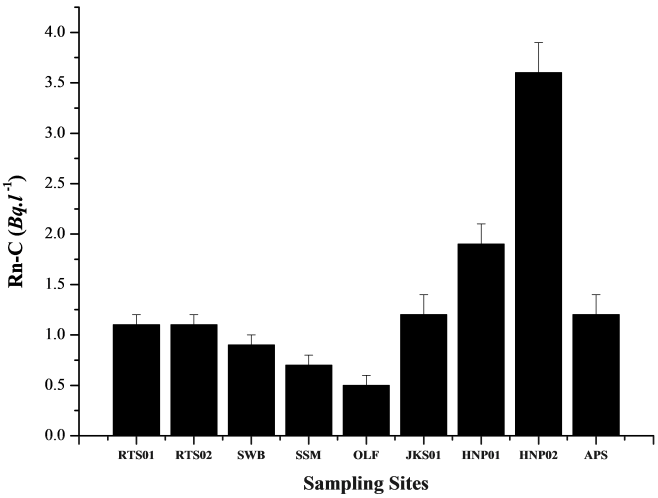

Figure 4.18: Radon Concentration in the water from the rivers in Pretoria Central and the South.

The radon concentrations measured from the rivers on western side of Pretoria, i.e. from JKS01 to APS in Figure 4.18 were generally higher than the South-Eastern side of the city. The distribution of radon concentration measured ranged from 0.5 $\pm$ 0.1 to 3.6 $\pm$ 0.3 as shown in Table 4.10.

4.6.3 Measurement along the rivers in Pretoria East

Table 4.11 shows the measured radon concentrations from the Pretoria East side of the Gauteng Province with the highest recorded concentration in this the current study of 4.9 $\pm$ 0.3 Bq.l^{-1} in Moreleta. Generally, the results in Table 4.11 show that radon concentration is higher as compared to the other parts of the province with an average radon concentration of 3.0 $\pm$ 0.2 Bq.l^{-1} which is higher that the provincial average radon concentration by a factor of 2.

Table 4.11: Radon Concentration and effective dose rate from the rivers in Pretoria East.

Sample ID	Description (River Name)	RH (%)	T (°C)	C_{Waterl} (Bq.l^{-1})	ED_{ing} (μSv.a^{-1})
EDN	Edendalspruit	19.4	21.9	2.6 ± 0.2	19.0
ZWP	Zwavelpoortspruit	23.5	25.4	1.8 ± 0.2	13.3
MRT	Moreleta	22.2	25.5	4.9 ± 0.3	36.1
PNS	Pienaarsriver	23.5	24.1	2.8 ± 0.2	20.7

4.7 Repeated Sample Points

The results of radon concentrations in the water samples from Hennops and Walkerspruit Rivers are presented in Table 4.12. The purpose of this exercise was to measure the radon concentration at the same spot in different days and time to check if there would be any difference. The results show the concentration of radon in Hennops River's sampling point was more stable with the variance of about 4 % between the 5^{th} and the 10^{th} of July 2014 while the sampling spot on the Walkerspruit showed a variation of about 24 % along the same period. The results show that all samples measured from Hennops River and Walkerspruit River were found to be below the MDL of the RAD-7 instrument used.

Table 4.12: The following samples were collected from the same place on different days. Two sampling places were recorded as the Hennops River and Walkerspruit in Pretoria.

Sample date	Description	RH (%)	T (°C)	C_{Waterl} (Bq.l^{-1})
5 July	Hennops	26	20.7	0.23 ± 0.05
5 July	Walkerspruit	24	18.7	0.31 ± 0.05
10 July	Hennops	19	24.8	0.24 ± 0.05
10 July	Walkerspruit	23	23.2	0.25 ± 0.06

4.8 Radon Concentration in the Commercial Bottled Water

The results of radon concentration in some well-known brands of bottled water in South Africa, presented in Table 4.13 were obtained with standard protocols WAT250 of the RAD-7 instrument. The main idea was to verify the quality of bottled mineral water regarding the concentration of radon.

Table 4.13: General survey of radon concentration from commercial (bottled) water.

Sample no.	Description	C_{Water} (Bq.l^{-1})	D_{water} μSv.a^{-1}
1	Distilled	0.3 ± 0.3	1.8 ± 1.1
2	Bonaqua	0.4 ± 0.2	1.7 ± 0.9
3	Valpre	0.7 ± 0.4	2.6 ± 1.4

The minimum detectable limit (MDL) of the RAD-7 instrument used in the current study was 0.4 Bq.l^{-1}. The results show that the three bottled water samples presented in Table 4.13 were found to be below or near to the MDL, respectively. Therefore, the ^{222}Rn concentration in mineral water as shown were below the the limit of 1 Bq.l^{-1} established by WHO (2011) [88].

5 Discussions

5.1 Quality Assurance for the Detector

It was necessary to subject the detector of choice in the current study, the RAD-7 instrument to a comparison test with the LSC using the standard sample. The response of the RAD-7 instrument was observed to be closely matched with that of the standard sample concentrations (see Table 4.1). The inter-comparison experiments gave confidence in the use of the RAD-7 instrument for radon concentration measurements in the laboratory and also in the field. The RAD-7 instrument was found to be a reliable and highly-sensitive detector for radon determination in the water. The measured radon concentration in river water is affected by a number of environmental factors which also play a major role in the radon release-rate into the atmosphere. Most critical among these factors is the sampling technique, see Section 3.2, including the choice of the sample size, counting time, meteorological parameters and temperature effects as disccussed below.

The study conducted (Csige *et al.*) using the RAD-7 instrument to measure the thoron concentration in solid building material by varying sample height h [87] was adopted in the current investigation by varying the (h) in the vial. Both studies showed that an increase in sample height, h, results in more apparent radon concentrations in the water sample (Figure 4.7). The sample height in the vial was increased by 1 mm from 1 mm to 5 mm (see Table 4.4). This exercise was useful for the determination of the radon release from a single measurement at the optimal sample thickness between 0.04 m and 0.06 m.

The internal temperature (T_{int}) and bias voltage affect the measurement of radon concentration when using the RAD-7 detector. Inside the detector, electronic noise is caused by heat resulting in peak tailing as shown in the energy spectrum, Figure 3.2a [85]. The effects of the T_{int} inside the detection chamber are shown in Table 4.5 and Figure 4.8b. An increase in T_{int} inside the detector compromised its counting efficiency. The performance and characteristics of the electrostatic collection rate of ^{222}Rn by the detectors are dependent on the charge of the uranium progeny atoms. In the RAD-7 detector, a high electric field of 2 keV in the detection chamber propels the positively charged ^{218}Po and ^{214}Po, onto the detector [98], (see Figure 3.2). The movement can be hindered by an increase in relative humidity, *RH*, inside the detection chamber. The theory of meteorological parameters which influence the effect of radon concentration agreed well with the measurements and confirmed the good functionality of the detector. These observations in the current study were also demonstrated by Stojkovic et al. [74].

The current study showed that in order to optimize the detector to measure the concentration of radon in water, agreed with P. Tuccimei *et al.* (2006), "he experimental conditions should be properly fixed and strictly respected because the values of exhalation rates are strongly variable and dependent on factors like sample volume, sample size, relative humidity, air temperature, water sample temperature" [96].

5.2 Radon Concentration from the Rivers in Gauteng

The study was performed to measure the level of elevation of radon concentration due to the mining activities in the Gauteng Province. In Table 4.6 the measured variations of radon concentrations in some of the Gauteng rivers can be observed. The results in Table 4.6 show that the average concentrations of ^{222}Rn in river water in the Gauteng Province is lower than the international levels ranging from 0.1 ± 0.1 to 4.9 ± 0.3 Bq.l^{-1} with an overall average of 1.4 ± 0.4 Bq.l^{-1}. The radionuclide specific concentration was found to be below WHO's guidance levels of 100 Bq.l^{-1} for ^{222}Rn in the water [17]. The USEPA (USA) has proposed a radon limit in water of 11.1 Bq.l^{-1} whereas Poland and the Czech Republic rec-

ommended contaminant levels of 75 Bq.l^{-1} and 50 Bq.l^{-1}, respectively [19]. The reason for the low radon concentration in the rivers or surface water could be due to its rapid dispersion into the atmosphere.

The results further showed that the radon concentration in the Klip and Jukskei Rivers (0.5 $\pm$ 0.1 and 1.2 $\pm$ 0.2 Bq.l^{-1}, respectively) which originate from the City of Johannesburg which is surrounded by the mines dumps and where they would be expected to have elevated concentrations of radon were found to be lower than the rivers in the Northern part of the province such as Hennops and Moreleta Rivers (3.4 $\pm$ 0.6 and 4.9 $\pm$ 0.3 Bq.l^{-1}, respectively) in Pretoria. The reason of the rivers that are far from the mine activities to have more radon concentrations than those in the nearby, could be characterized by the level of ^{238}U in soil and bedrock. The highest recorded radon concentration in Pretoria and in Johannesburg were 1 Bq.l^{-1} and 0.5 1 Bq.l^{-1} , respectively.

It was observed that in the radon concentrations increased downstream (see Figures 4.13 and 4.14 for the Jukskei River, Hennops River and Walkerspruit River, and a weighted mean activity concentration of ^{222}Rn of 0.99 Bq.l^{-1} was measured. The results show the variation of measured radon concentrations increased by a factor of 5, ranging from 0.4 $\pm$ 0.2 in Bezuidenhout valley (Johannesburg) to 2.3 $\pm$ 0.4 in Kyalami (about 30 km north of Johannesburg). The difference in concentration might be due to the geological nature of the bedrocks of the river. Figure 4.15 shows the regional percentage contribution of ^{222}Rn to the total radon concentrations measured in the province. The Northern and the North-eastern regions of the Gauteng Province contributed 77.2 % whilst the Southern and the Western parts of the province had 22.8 %.

The measured annual effective dose values at the sampling areas as presented in Table 4.6 ranged from 0.9 to 36 μSv.a^{-1} with an average value of 10.3 $\pm$ 8.6 μSv.a^{-1}. The highest measured effective dose rate values were 19, 20, 21, 25 and 36 μSv.a^{-1} from Edendalspruit, Pienaarsriver, Natalspruit and Hennops Moreleta rivers respectively. However, all the measured values of the annual effective dose in Table 4.6 are below the background of 460 μSv.a^{-1} [89].

Figure 4.11 shows that the mine dumps have little influence in the elevation of radiation concentration in rivers as might be expected. The radon concentration hotspots in rivers are not correlated to drainage of mining areas, therefore the data is consistent with an interpretation that local natural geological conditions are more pertinent than anthropological considerations. “Mining accelerates natural geological processes by transferring radioactive materials from underground to tailings dams on surface. Water plays an important role in moving naturally occurring radionuclides in underground water to surface. Where mines have uranium, there is, in addition, significantly enhanced scope for uranium and radium, mobilised during the leaching process, to escape into the environment via water streams” (G. Wendel, 1998) [97]. As far as radon is concerned, rivers soon lose the memory of the radon distribution of their origin. The local concentration of radons parents and the potential of its host material to release this radon become the dominant factors.

While it was necessary for the current study to measure the radon concentration levels in the rivers around mining activities, it was also important to compare with those rivers that do not originate from or near the mining areas. According to the findings of the study, there were no indication of influence by anthropogenic activity to the elevated radon concentration. However, it will be interesting for the future studies to link between the regional geological setup and the general radiological levels, particularly of radon in natural water, and its impact on the safety of general public with respect to this source.

6 Conclusions

6.1 Conclusions

The following conclusions were reached about the technique which was applied for the current study:

- Meteorological parameters conditions should be carefully fixed and be respected because the radon release rates dependends on factors like sample volume, sample size, relative humidity, internal cell temperature, water sample temperature [96].

- The $\alpha-$spectrometry technique as applied by the RAD-7 instrument was shown to be appropriate for determination of radon concentrations.

The results obtained from the current study of general survey of radon concentration in some rivers of Gauteng Province led to the following observations:

- The presence of radon concentration in the surface water (rivers) in Gauteng is not correlated in intensity to areas which drain the regions where there are mining activities.

- It is possible other NORM isotopes, not as mobile as radon, might accumulate more due to anthropogenic activities, but radon less so as it is too rapidly released from water.

- Since the current study showed the radon concentration in rivers is not significantly increased due to anthropogenic activities, it is likely that natural

sources are the most significant for accounting for the observed radon concentrations [13].

- The average radon concentration measured in the Gauteng Province rivers was found to be below the international acceptable levels for radon concentration in water as recommended by the United States Environmental Protection Agency (USEPA) and the World Health Organisation (WHO), which was consistent with C. Cosma *et al.*[12, 13].

- The level of radon concentration measured in the current study does not pose a health problem to the public.

6.2 Recommendations

- This study is one of a few surveys of environmental radon, in South Africa particularly in rivers. It is very important to have more radiological research performed in order to develop a radiological map for the whole country.

- Awareness is needed about the danger that can be caused by exposure to excess radiation, particularly South African citizens who stay near the mines.

- More general studies of NORMS as radon in water appears to be less of a problem.

- Studies of radon in air and in water much nearer to the mines.

- Studies of radon in materials made from mine waste.

7 Appendix

7.1 Appendices

Table 7.1: Varying sample concentration.

Vial no.	V_{oil} (ml)	V_{LSC} (ml)	Rn-C_{LSC} (mBq/l)	V_{water} (ml)	V_{RAD-7} (ml)	Rn-C_{RAD-7} (mBq/l)
A	9.90	10.02	32.77 ± 28	10.00	10.03	74.04 ± 18
B	9.81	10.00	64.98 ± 20	10.02	10.78	111.11 ± 25
C	9.77	10.02	106.6 ± 15	10.10	10.02	148.44 ± 23
D	9.81	10.03	200.94 ± 11	10.01	10.04	259.55 ± 53

Table 7.2: The effects of sample volume on radon concentration of a river sample.

Vial No	Time (min)	V_{sample} (ml)	V_{air} (ml)	Low (mBq/l)	High (mBq/l)	Rn-C_{RAD-7} (mBq/l)
A	72	140	110	0.15	1.64	0.49 ± 0.43
B	192	150	100	0.45	1.34	0.95 ± 0.27
C	300	160	90	0.60	2.23	1.23 ± 0.46
D	382	170	80	0.89	2.23	1.42 ± 0.41
E	460	180	70	0.74	2.09	1.60 ± 0.42

Table 7.3: The effect of *RH* and internal temperature on the counting efficiency of the RAD-7 during the measurement period.

Measurement time (min)	T_{int} (°C)	RH (%)	Rn-C_i (mBq/*l*)	Rn-C_f (mBq/*l*)
5.00	20.55 ± 1.82	13.09 ± 1.82	34.22 ± 8.14	33.46±7.10
13.00	20.98 ± 0.21	17.64 ± 1.13	33.79 ± 9.41	33.04±9.20
21.00	21.45 ± 0.16	20.50 ± 0.53	31.49 ± 7.40	33.46±6.37
32.00	22.01 ± 0.28	22.36 ± 0.51	29.72 ± 7.16	32.28±6.17
36.00	22.35 ± 0.17	24.00 ± 0.50	26.60 ± 1.50	29.47±1.29

Table 7.4: Effects of meteorological parameters on radon concentration.

t (min)	RH (%)	T (°C)	Rn (mBq/*l*)
4	31.00 ± 1.83	23.25 ± 0.30	1.11 ± 0.48
8	29.50 ± 1.29	23.85 ± 0.17	1.39 ± 0.48
12	28.00 ± 0.82	24.00 ± 0.00	2.23 ± 1.74
16	27.25 ± 0.96	24.08 ± 0.15	3.61 ± 0.96

Table 7.5: The influence of Relative Humidity (*RH*) and internal temperature (T) on the standard sample.

Vial no.	Standard sample	RAD-7 (mBq/*l*)	RH (%)	Δ RH (%)	r_{RH}	T (°C)	Δ T (°C)	r_T
A	92.06	90.66	31	4	-0.894	23.3	0.6	-0.814
B	178.46	135.99	29.5	3	-0.947	23.9	3	-0.707
C	262.59	181.33	28	2	-0.999	24	-	-
D	336.97	314.65	27.3	2	-0.51	24.08	2	0.814

Table 7.6: Time-variation for RAD-7 equilibrium.

Counting no.	Time (min)	RH (%)	T_{RAD-7}	Rn-C_{RAD-7} (mBq/l)
1	5	13	23.7	1.34 ± 1.24
2	10	14	23.7	0.89 ± 1.08
3	15	15	23.7	1.19 ± 1.19
4	20	16	24	1.64 ± 1.33
5	25	17	24	1.49 ± 1.28
6	30	17	24.3	1.04 ± 1.14
7	35	18	24.3	1.34 ± 1.24
8	40	18	24.3	0.60 ± 0.95
9	45	19	24.6	0.74 ± 1.03
10	50	19	24.6	2.23 ± 1.49
11	55	20	24.9	0.74 ± 1.03
12	60	20	24.9	1.49 ± 1.28

Table 7.7: Radiation dose ranges for drinking water with health effects and intervention decision time frames indicated (DWAF, 2002).

Dose class/colour	Dose range (mSv/a)	Health effects	Intervention decision time frame
Class 0 (Blue, ideal water quality)	0.01 – 0.1	No observable health effects	Intervention not applicable
Class 1 (Green, good water quality)	>0.1 – 1	No observable health effects. Typical range of worldwide natural dietary ingestion from water and food.	No intervention required, but ALARA principle applies (keep dose as low as reasonably achievable)
Class 2 (Yellow, marginal water quality)	>1 – 10	Small increase in cancer mortality risk	Consider intervention within 2 years
Class 3 (Red, poor water quality)	>10 – 100	Cancer risk statistically detectable in very large population groups	Intervention required within within 1 year
Class 4 (Purple, unacceptable water quality)	>100	Health effects clinically detectable	Immediate intervention required

Table 7.8: Radon concentration build-up on Jukskei River (from Johannesburg to Midrand).

Sample no.	Description sampling spot	RH (%)	T (°C)	C_{Waterl} (mBq/l)	C_{Actual} (mBq/l)	D_{water} mSv.a^{-1}
1	JHB Bruma	23.5	22	0.35 ± 0.21	0.39 ± 0.21	1.28 ± 0.77
2	Bruma Lake	22.5	26.3	0.35 ± 0.24	0.39 ± 0.26	1.42 ± 0.95
3	Edenvale	21.5	21.4	0.94 ± 0.34	1.04 ± 0.37	3.80 ± 1.35
4	Edenvale Hosp	20	26	1.40 ± 0.50	1.54 ± 0.55	5.62 ± 2.01
5	Mooderfontain	20	26	1.58 ± 0.50	1.74 ± 0.55	6.35 ± 2.01
6	Shakespear	19	24.8	1.48 ± 0.48	1.63 ± 0.53	5.95 ± 1.93
7	Alexandra	23	23.2	0.45 ± 0.23	0.50 ± 0.25	1.83 ± 0.91
8	Bucleugh	24	18.7	0.58 ± 0.33	0.64 ± 0.36	2.34 ± 1.31
9	N1 Bridge	26	20.65	0.81 ± 0.47	0.89 ± 0.52	3.25 ± 1.90
10	Waterfall	26.5	23.9	1.66 ± 0.22	1.83 ± 0.24	6.68 ± 8.76
11	Woodmead	18	24.2	3.23 ± 0.92	3.56 ± 0.41	5.22 ± 1.50
12	Kyalami Bridge	20.5	19.2	1.30 ± 0.37	1.43 ± 0.41	4.73 ± 1.42

Table 7.9: General survey of radon concentration from the rivers in Pretoria.

Sample no.	Description (River Name)	RH (%)	T (°C)	C_{Waterl} (mBq/l)	C_{Actual} (mBq/l)	D_{water} μSv.a^{-1}
1	Apies	16	20.3	0.56 ± 0.31	0.61 ± 0.34	2.23 ± 1.24
2	Swart-spruit	23.5	22	0.45 ± 0.24	0.50 ± 0.27	1.83 ± 0.99
3	Moganwe	22.5	26.3	1.01 ± 0.40	1.11 ± 0.44	4.05 ± 1.61
4	Saulsville	21.5	21.4	1.49 ± 0.44	1.64 ± 0.49	5.99 ± 1.79
5	Atteridgeville	20	26	1.53 ± 0.51	1.68 ± 0.57	6.13 ± 2.08
6a	Walkerspruit	24	18.7	3.12 ± 0.75	3.44 ± 0.83	1.26 ± 3.03
6b	Walkerspruit	19	24.8	2.51 ± 0.59	2.78 ± 0.64	1.01 ± 2.34
7a	Hannops (Lake)	26	20.65	2.29 ± 0.50	2.52 ± 0.55	9.20 ± 2.01
7b	Hannops (N14)	23	23.2	2.40 ± 0.50	2.62 ± 0.56	9.56 ± 2.04
8	Sesmylspruit (Irene)	22	18.5	0.62 ± 0.25	2.52 ± 0.55	9.20 ± 2.01
9	Moreleta (PTA East)	21	20.2	0.72 ± 0.35	0.79 ± 0.39	2.88 ± 1.42
10	Edendalspruit (Mamelodi)	20	20.3	0.77 ± 0.40	0.85 ± 0.44	3.10 ± 1.61
11	Pienaarsriver (Mahube)	19.4	22.2	0.53 ± 0.23	0.58 ± 0.25	2.12 ± 0.91
12	Skinnerspruit (PTA West)	23	23.6	0.33 ± 0.18	0.36 ± 0.20	1.31 ± 0.73

8 Publications

8.1 Published paper from the current study

Masevhe *et al*., J Environ Anal Toxicol 2017, 7:4
DOI: 10.4172/2161-0525.1000472

References

[1] J-M. Lee and G. Kim. *A simple and rapid method for analysing radon in coastal and ground waters using a radon-in-air monitor*. Journal of Environmental Radioactivity, vol 89, pp. 219 – 228, 2006.

[2] K.H. Ali, R.H. Abdu and R.S. Ahmed. *Measurement of radon concentration in soil gas using RAD-7 in the environs of Al-Ashraf City-Iraq*. Advances in Applied Science Research Palagia Research Library, vol 2(5), pp 273 – 278, 2011.

[3] A. Binesh, H. Arabshahi and Z. Pourhabib. *Radioactivity and dose assessment of heavy radioactive pollution, radon and radium from water sources of 3 northern regions in Iran*. International Journal of Physical Sciences, vol 6(35), pp. 7969 – 7977, 2003.

[4] S. Singh, A. Kumar, B.S. Bajwa, S. Mahajan, V. Kumar and S. Dhar. *Radon monitoring in soil gas and groundwater for earthquake prediction studies in North West Himalayas, India*. Terr. Atmos. Ocean. Sci., Vol. 21, No 4, pp. 685 – 695, August 2010.

[5] H.A. Khan. *Radon: a friend or a foe?* International Journal of Radiation Application and Instrumentation. Part D. Nuclear Tracks and Radiation Measurements, vol 19 (1 - 4), pp. 353 – 362, 1991.

[6] S.M. Abo-Elmagd, S.A. El-Fiki and E. Salama. *Passive and active measurements of radon-related parameters inside ancient Egyptian tombs in Luxor*. Science Direct. Radiation Measurements, vol 42, pp. 116 – 120, 2007.

[7] S. Darby, D. Hill, A. Auvinen, J. Barros-Dios, H. Baysson, F. Bochicchio, H. Deo, R. Falk, F. Forastiere, M. Hakama, I. Heid, L. Kreienbrock, M. Kreuzer, F. Lagarde, I. Mkelinen, C. Muirhead, W. Oberaigner, G. Pershagen, A. Ruano-Ravina, E. Ruosteenoja, A. Rosario, M. Tirmarche, L. Tomsek, E. Whitley, H. Wichmann and R. Doll. *Radon in homes and risk of lung cancer: collaborative analysis of individual data from 13 European case-control studies.* British Medical Journal, vol. 330, No. 7485, pp. 223 – 228, 2005.

[8] H. Al Zabadi, S. Musmar, S. Issa, N. Dwaikat and G. Saffarini. *Exposure assessment of radon in the drinking water supplies: a descriptive study in Palestine*. BMC Res Notes. 2012; 5: 29. Published online 2012. doi: 10.1186/1756-0500-5-29, 2012.

[9] S.A. Talha, R.J. de Meijer, R. Lindsay, R.T. Newman, P.P. Maleka and I.N. Hlatshwayo. *In-field radon measurement in water: novel approach*. Journal of Environmental Radioactivity, vol. 101 (12), pp. 1024 – 1031, 2010.

[10] H. Zeeb and F. Shannoun. *WHO handbook on indoor radon: a public health perspective*. WHO Library Cataloguing-in-Publication Data, ISBN 978 92 4 154767 3, 2009.

[11] D.M. Bonotto and C.B. Mello. *A combined method for evaluating radon progeny in waters and its use at Guarani aquifer, Sao Paulo State, Brazil*. J. Environ. Radioact, vol 69, pp. 21 – 35, 2006.

[12] C. Cosma, M. Moldovan, T. Dicu and T. Kovacs. *Radon in water from Transylvania (Romania)*. Radiation Measurements, vol 43(8), pp. 1423 – 1428, 2008.

[13] S. Grlonder and S. Karnbranslehantering. *Analysis of radioactive isotopes in near surface groundwater, surface water, biota and soil*. Per Roos, Riso National Laboratory, pp. 9 – 66, 2009.

[14] M. Schubert, W. Buerkin, P. Peña, A.E. Lopez and M. Balcázar. *On-site determination of the radon concentration in water samples: Methodical*

background and results from laboratory studies and a field-scale test. Radiation Measurements vol 41(4), 492 – 497, 2006.

[15] P. Manders, L. Godfrey, P. Hobbs. *Acid Mine Drainage in South Africa*. CSIR Researchers on current research developments, social, enviroments and policy topics.

[16] R. Kleinschmidt. *Radioactive residues associated with water treatment, use and disposal in Australia*. Eprints.edu.au/48058/1/Ross-Kleinschmidt-Thesis.pdf, Queensland University of Technology, pp. 11.

[17] G.C. Irina, L. Olivier, P. Nathalie, L Dominique and D. Isabelle. *Health Effects of Naturally Radioactive Water Ingestion: The Need for Enhanced Studies*. Environ Health Perspect; vol 119(12), pp. 1676 – 1680, 2011.

[18] I. Guseva, O. Laurent, N. Pires and I. Dublineau. *Health effects of naturally radioactive water ingestion: The need for enhanced studies*.Environmental Health Perspective, vol. 119, pp. 1676 – 1680, 2011.

[19] J. Wiltse and V.L. Dellarco. *U.S. Environmental Protection Agency guidelines for carcinogen risk assessment: Past and future*. NCEA-F-0644, vol 265(1 - 3), pp. 3 – 15, 1999.

[20] DWAF, NRMP. *Report on the radioactivity monitoring programme in the Klip River Catchment. National Monitoring Programme*. Report No., N000000REQ0403, Resource Quality Services, Department of Water Affairs and Forestry, Pretoria, South Africa, 2003.

[21] M.A. Nabil. *Measurement of radon concentration in soil at North Gaza*. Department of Physics, University of Athens, Greece. M.Sc. thesis, pp. 2 – 3, 2005.

[22] K. Jochen. *Decay chains and half-lives of the three natural radioactive families*. Naturally occurring radioactive material. Data taken from Karlsruher Nuklidkarte, 1998.

[23] O. Maxwella, H. Wagirana, N. Ibrahimb, S.K. Leec and S. Sabrid. *Radiological Monitoring of Borehole in Dei-Dei, Abuja, North Central Nigeria* . 5th International Conference on Environmental Science and Development – ICESD 2014, vol 10, pp. 54 – 58, 2014.

[24] M. Cuk, P. Papic and J. Stojkovic. *Natural radioactivity of groundwater in Serbia*. Annales Geologiques de la Peninsule Balkanique. Belgrade, vol 74, pp. 63 – 70, 2013.

[25] L. Tommasino. *Radiochemical methods— radon*. Encyclopedia of Analytical Science (Second Edition) pp. 32 – 44, 2013.

[26] A.H. Leuschner, D. van As, A. Grundling and A. Steyn. *A survey of the indoor exposure to radon in South Africa*. The Clean Air Journal Journal ISSN 0379 – 4709.

[27] M.F. LÁnnunziata. *Radiation and Radiological Decay.* Handbook of Radioactivity Analysis. Third Edition. Academic Press in an imprint of Elsevier, pp. 659 – 660, 2012.

[28] F.H. Attix. *Introduction to radiological physics and radiation dosimetry*. Wiley-VCH Verlag GmbH, Weinheim, Germany. Chapter 5: Absorbed dose in radioactive media, 2007.

[29] E. Annex. *Sources-to- effects assessment for radon in homes and workplace, In: effects of ionizing Radiation*. United Nations Scientific Committee on the Effects of Atomic Radiation UNSCEAR Report to the General Assembly, vol 2, United Nation, New York, 2008.

[30] S. Lorenz, T. Kaudse and W. Aeschbach-Hertig. *F50/51 Limnophysics*. Physics of Aquatic Systems, Institute of Environmental Physics in Heidelberg, Voslesungsskript, March, 2011.

[31] K.S. Krane. *Introductory Nuclear Physics.* Library of Congress Cataloging in Publication Data. John Wiley & Sons. Oregon State University. Rev. ed. of Introductory nuclear physics/David Halliday. 2nd. ed, 1955.

[32] B. Annex. *Exposure of the public and workers from various sources of radiation, In: Sources and Effects if Ionizing Radiation*. United Nations Scientific Committee on the Effects of Atomic Radiation UNSCEAR 2008 Report to the General Assembly. Volume I, United Nation, New York, 2008.

[33] L. Salonen, L Kaihola, B.C. Gordon, T.C. Charles and J. Passo Jr. *Chapter 9: Environmental liquid scintillation analysis*. Handbook of Radioactivity Analysis (Third Edition), pp. 265 – 693, 2012.

[34] K. Horiuchi, T. Ishii and M. Kobayashi. *Liquid Scintillation Counting measurements of radon from seepage groundwater in Lake Biwa, Japan*. In: J.E. Noakes, F. Schoonhofer and H.A. Polach (Eds.), Liquid Scintillation Spectrometry. Radiocarbon Publishers, University of Arizona, Tucson, pp. 383 – 390, 1992.

[35] S. Purkl and A. Eisenhauer. *Determination of Radium isotopes and ^{222}Rn in a groundwater affected coastal area of Baltic Sea and the underlying sub-sea floor aquifer*. Marine Chem. vol 87, pp. 137 – 149, 2004.

[36] P.G. Cook, G. Favreau, J.C. Dighton and S. Tickel. *Determination of natural groundwater influx into a tropical river using radon, chloroflourocarbons and ionic environmental tracers*. J. Hydrol. vol 277, pp. 74 – 88, 2003.

[37] S. Lamontagne, C. Le Gal La Salle, G. Hancock, I.T. Webster, T. Craig, C.T. Simmons, A.J. Love and J-S. Julianne. *Radium and radon radioisotopes in regional groundwater, intertidal groundwater, and seawater in the Adelaide coastal waters study area: implications for the evaluation of submarine groundwater discharge*. Marine Chem, vol 109, pp. 318 – 336, 2008.

[38] C.Y. King. *Radon Monitoting for Earthquake Prediction in China*. Earthquake Pred. Res. vol 3, pp. 47 – 68, 1985.

[39] C.R. Cothern and J.E. Smith. *Environmental radon*. Environmental Science Research, Published by Springer US, vol. 35, 1987.

[40] M. Wilkening. *Radon in the environment*. Studies in Environmental Science, vol 40, 1990.

[41] Mueller Asssociates, Inc. *Handbook of radon in buildings: detection, safety, and control*. Hemisphere Publishing Corporation, SYSCON Corporation, Brookhaven National Laboratory, 1988.

[42] R.C. West. *CRC Hanbook of Chemistry and Physics*. 60th Eition. Boca Raton, FL: CRC Press, pp. 1979 – 1980, B-19, 1980.

[43] J. Singh, H. Singh, S. Singh and B.S. Bajwa. *Estimation of uranium and radon concentration in some drinking water samples*. Radiation Measurements, vol 43, Supplement 1, pp. S523 - S526, 2008.

[44] L. Stein. *Chemical properties of radon, and its decay products*. American Chemical Society, pp. 240 – 251, 1987.

[45] M.C. Galletti. *New gamma-ray Spectrometry methods for estimating K, U, Th concentrations in rocks of the Sardinia Batholith*. Via Muroni 25, I-07100 Sassari, Italy. University of Sassari PhD School in Natural Science, 2013.

[46] H.M. Prichard, T. F. Gesell and C.R. Meyer. *Liquid Scientillation Analyses for radium-226 and radon-222 in potable waters, Liquid Scintillation Counting*. Recent Applications and Development, vol. 1, pp. 347 – 355, Physical Aspects.

[47] A. Rybalkin. *Numerical and analytical assessment of radon diffusion in various media and potential of charcoal as radon detector*. The University of Utah, pp. 13 – 14, 2012.

[48] T. Tuukka. *Radon and radium in well water: Measurements and mitigation of exposure*. STUK-A255. Helsinki, pp. 102, 2013.

[49] W.S. Snyder and J. Neufeld. *On the passage of heavy particles through tissue*. Radiation Research 1957; 6: pp. 67 – 78, 1957.

[50] *Wikipedia: The free encyclopedia* (2017, January 17). Wikimedia Foundation, Inc. Retrieved January 15, 2017, from `http://en.wikipedia.org/wiki/Bethe_formula`, 2007.

[51] J. Durham. *Concepts, quantities, and dose limits in radiation protection dosimetry*. The 2nd Summer School on Solid State Dosimetry: Concepts and Trends in Medical Dosimetry. Volume 41 (1), pp. S28 – S35, 2006.

[52] S.A. Durrani and R. Ilic. *Radon Measurements by Etched Track Detectors*. World Scientific, 1997.

[53] A.T.A. Siddig and R. Lindsay. *Measurements and Applications of Radon in South African Aquifer and River Waters*. The University of the Western Cape, Thesis, pp.23 – 24, 2009.

[54] T. di Dottorato. *Indoor and outdoor natural radioactivity in the Vulsini Volcanic District (Central Italy): estimation of doses and radiological risks*. Ciclo di Studi, pp. 26 – 27, 2011.

[55] T. Kluge. *Tracing and quantifying groundwater inflow into lakes using a simple method for radon-222 analysis*. Hydrol. Earth Syst. Sci. vol 11, pp. 1621 - 1631, 2007.

[56] L.D. Cecil and J.R. Green. *Environmental tracers in subsurface hydrology; Chapter 6: Radon-222*. US Geological Survey, Idaho Falls, USA, pp. 175 – 194, 2000.

[57] M. Alegria. *Measuring the Radiosensitivity of healthcare personnel in radiation-based medical diagnosis and treatment*. Seguridad y Medio Ambiente, Year 34 N^o 134 Second Quarter 2014.

[58] C. Eisenhart. *Realistic evaluation of precision and accuracy of instrument calibration systems*. J. Res. 67C, pp. 161 – 187, 1963.

[59] S.M. Seltzer and M.J. Berger. *Evaluation of the collision stopping power of elements and compounds of electron and positron*. Int. J. Appl. Radiat. Isot. vol 33, pp. 1189 – 1218, 1982.

[60] W.M. Snow, Z. Chowdhuri, M.S. Dewey, X. Fei, D.M. Gilliam, G.L. Greene, G.S. Nico, H. Sorensen and H.H. Anderson. *Stopping power of Al, Cu, Ag, Pb and U for 5 18 MeV protons and deuterons*. Phys. Rev. vol 8B, pp. 1854 – 1863, 1973.

[61] G.F. Knoll. *Radiation detection and measurements*. Fourth edition. J. Wiley and Sons, New York, pp.830, 2008.

[62] ISO/IEC 17025.*General requirements for the competence of testing and calibration laboratories*. Second edition, 2005.

[63] IAEA. *A Combined Procedure for Determination of Plutonium Isotopes,* ^{241}*Am and* ^{90}*Sr in Environmental Samples*. International Atomic Energy Agency, Vienna, 2012; `http://nucleus.iaea.org/rpst/ReferenceProducts/AnalyticalMethods/index.html`, 2012.

[64] M. Saito. *Correction for loss of radon-222 in water sample caused by the use of a polyethylene bottle*. Radioisotopes vol 32(3), pp. 109 – 112, 1983.

[65] L. Zikovsky and N. Roireau. *Determination of Radon in Water by Argon purging and alpha counting with prportional counter*. Appl. Radiat. Isot. 41, pp. 679 – 681, 1990.

[66] T. Yanliang and X. Detao. *Revision for measuring the radon exhalation rate from the medium surface*. IEEE Transactions on Nuclear Science. Vol, 58(1), 2011.

[67] RAD-7, RAD H_2O. *Radon in Water Accessory*, DuRRIDGE Co., user manual, pp. 31 – 48, 2012.

[68] D. Guida, M. Guida, D. Guadagnuolo, A Cuomo and V. Siervo. *Using Radon-222 as naturally occurring tracer to investigate the streamflow-groundwater interactions in typical Mediterranean fluvial-karst landscapes: interdisciplinary studies in the Campania region (southern Italy).* 12^{th} European Geoparks Conference, Natioanl Park of Cilento, Vallo di Diano and Alburni Geopark (Third Edition), pp. 104 – 109, 2013.

[69] N. Vajda, P. Martin and C. Kim. *Chapter 6 - Alpha Spectrometry*. Handbook of Radioactivity Analysis (Third Edition), pp. 363 – 422, 2012.

[70] N. Vajda. *Up to date radiochemical methods for the determination of long lived radionuclides in the environment*. Journal of Analytical Science and Technology, vol 2 (Appl A), pp. A108 – A114, 2011.

[71] D-W. Hwang, I-S. Lee, M. Choi and T-H Kim. *Estimating the input of submarine groundwater discharge and derived nutrients in Geoje Bay, Korea using ^{222}Rn-Si mass balance model*. Marine Pollution Bulletin, vol. 110(1), pp. 119 – 126, 2016.

[72] M.D. Alenezy. *Radon concentrations measurement in Aljouf, Saudi Arabia using active detecting method*. Natural Science, vol 6, pp. 886 – 896, 2014.

[73] N.U. Khattak, M.A. Khan and M.T. Shah. *Radon concentration in drinking water sources of the main campus of the University of Peshawar and surrounding areas, Khyber Pakhtunkhwa, Pakistan* . Jouranl of Radiology-analytical and Nuclear Chemistry, vol 290(2), pp. 493 – 505, 2011.

[74] I. Stojkovic, B. Tenjovic, J. Nikolov, M. Veskovic, D. Mrda and N. Todorovic. *Improvement of measuring methods and instrumentation concerning ^{222}Rn determination in drinking waters - RAD-7 and LSC technique comparison*. Applied Radiation and Isotopes vol 98, pp. 117 – 124, 2015.

[75] Y. Kobayash. *Laboratory manual for Liquid Scintillation Counting*. PACKARD (c) Instrument Co. Inc, 1988.

[76] Y. Ranebo, R. Pollanen, M. Eriksson, T. Siiskonen and N. Niagolova. *Characterization of radioactive particles using non-destructive alpha spectrometry*. Appl. Radiat. Isot. vol 68, pp. 1754 – 1759, 2010.

[77] C. *Samuelsson. Experts from the history of alpha recoils*. J. Environ. Radioact. 102, pp. 531 – 533, 2011.

[78] D. Kotze. *Radioactivity analysis of water*. Report no. RA-08894, Radio Analysis laboratory, Nuclear Energy Corporation of South Africa (Necsa), Pretoria, 2008.

[79] K.Md. Najeeb and N. Vinaychandran. *Radon contamination in groundwater and application of isotopes in groundwater studies*. Journal of Geological Science, India, vol 77, pp 481 – 482, 2010.

[80] D. van As, A. Grundling, S. Redding and R. Brits. *An assessment of the population dose due to radon-222 from mine tailings on the Witwatersrand*. Nuclear Development Corporation of South Africa (Pty) Ltd. Report on Population Dose (Radon-222) - Gauteng, 2007.

[81] GDARD. *Concept Study on Reclamation of Mine Residue Areas for Development Purpose*. Gauteng Department of Agriculture and Development, 2012. `http://www.gdard.gpg.gov.za/Documents1/GDARDMRAsStrategy2012110-color.pdf`, 2012.

[82] H. Cember and T.E. Johnson. *Introduction to Health Physics.* 4th Edition. New York: The McGraw-Hill Companies, Inc, pp. 86 – 89, 2009.

[83] M.D Alyce Bezman Tarcher. *Principles and practice of environmental medicine.* Springer Science and Business Media,School of Medicine, University of California, San Francisco, California.

[84] J.B.R. Battat, J. Brack, E. Daw and A. Dorofeev. *Radon in the DRIFT-II directional dark matter TPC: emanation, detection and mitigation*. Preprint typeset in JINST style - HYPER VERSION. arXiv:1407.3938v2 [physics.ins-det] 25 Aug 2014. pp. 10 – 11, 2014.

[85] M. Jalili. *Radiation Physics and Chemistry*. Vol 81, pp. 749 – 757, 2012.

[86] K.Y. Lee and W.C. Burnett. *Determination of air-loop volume and radon partition coefficient for measuring radon in water sample*. Published with open access at Springerlink.com on 21 May 2013. J. Radioanal Nucl Chem, vol 298, pp. 1359 - 1365, 2013.

[87] I. Csige, Z. Szabo and C. Szabo. *Experimental technique to measure thoron generation rate of building material samples using RAD-7 detector*. Radiation Measurements, pp. 1 – 4, 2013.

[88] J. Kappke, S.A. Paschuk, V. Deniak, J.N. Correa, M. Reque, C.G. Tabuchi, F. Del Claro1 and A.F. Perna. *Measurements of radon and radium activity in bottled mineral water*. International Nuclear Atlantic Conference - INAC, Recife, PE, Brazil, November 24 – 29, 2013.

[89] E. Marfo. *Study of the radiological impact of small-scale mining activities at Dunkwa-on-offin in the central region, Ghana*. A thesis for the Masters of Philosophy in Radiation Protection, University of Ghana, Legon, pp. 73 – 74, 2014.

[90] C.J. Voster. `http://www.geoscience.org.za/images/Maps/gauteng_activegoldmines.gif`, 2002.

[91] R. Engelbrecht. *Environmental radioactivity monitoring*. Handbook of Radioactivity Analysis (Third Edition), pp. 695 – 726, 2012.

[92] G. Cinelli. *Indoor and outdoor natural radioactivity in the Vulsini volcanic district (Central Italy): estimation of doses and radiological risks*. University of Bologna, Thesis, 2009 – 2011.

[93] S.A. Quinn. *Evaluation of a radiochemical method to estimate the rate of solute diffusion within a dual porosity Chalk aquifer*. Department of Earth Sciences, PhD Thesis, pp. 128 – 154, 2012.

[94] M. Schubert, A. Paschket, E. Lieberman and W. Burnett. *Air-water partitioning of ^{222}Rn and its dependence on water temperature and salinity*. Environmental Sciences Technology, vol. 46(7), pp. 3905 – 3911, 2012.

[95] B. Xu, W.C Burnett, D.Lane-Smith and Z. Yu. *A simple laboratory-based radon calibration system*. Journal of Radioanalytical and Nuclear Chemistry, vol. 283(2), pp. 457 – 463, 2010.

[96] P. Tuccimeia, M. Moronic and D. Norciaa *Simultaneous determination of ^{222}Rn and ^{220}Rn exhalation rates from building materials used in Central Italy with accumulation chambers and a continuous solid state alpha detector: Influence of particle size, humidity and precursors concentration*. Applied Radiation and Isotopes, vol. 283(64), pp. 254 – 263, 2006.

[97] G. Wendel. *Radioactivity in mines and mine water – sources and mechanisms*. The Journal of The South African Institute of Mining and Metallurgy, Avgold Limited, Hartebeestfontein Division, SA ISSN 0038223X/3.00 + 0.00, pp. 78 – 92, 1998.

[98] G. Kim. *Measurement and application of radium and radon in the environment*. Journal of Analytical Science and Technology, vol. 2(3), pp. 115 – 119, 2011.